STABILIZED ORGANIC CATHODES FOR ZINC-ION BATTERIES

DEVELOPMENT OF STABILIZED ORGANIC CATHODES VIA GRAFTING REDOX-ACTIVE MOLECULES TO CARBON IN AQUEOUS ZINC-ION BATTERIES FOR ENERGY STORAGE SYSTEMS

BY THOMAS J. BAKER, B.ENG.BIOSCI.

A Thesis Submitted to the School of Graduate Studies in the Partial Fulfillment of the Requirements for the Degree Master of Applied Science

April 17, 2024

McMaster University

Master of Applied Science (2024)

Hamilton, Ontario (Department of Chemical Engineering)

TITLE: Development of Stabilized Organic Cathodes via Grafting Redox-active Molecules to Carbon in Aqueous Zinc-ion Batteries for Energy Storage Systems

AUTHOR: Thomas J. Baker (McMaster University)

SUPERVISOR: Dr. Drew Higgins

NUMBER OF PAGES: xviii, 84

Lay Abstract

Renewable electricity production is necessary to mitigate climate change but the production of electricity through many renewables like wind and solar can vary significantly on any given day. Lithium-ion batteries are being explored for storing electricity for use on the grid, but they have many downsides including being flammable and expensive. Zinc-ion batteries are non-flammable and cost-effective alternatives to lithium-ion batteries. They are currently not as widely used as lithium-ion batteries because of their poorer performance. However, for storing electricity for power grids, with the correct selection of materials to make the battery, zinc-ion batteries can perform well enough to compete with lithium-ion batteries. This work investigates a modification of a material used in zinc-ion batteries, that allows the battery to maintain a higher capacity after many charge and discharge cycles.

Abstract

To combat climate change, governments have pledged to become more dependent on renewable electricity production. However, the intermittency of renewable power generation requires modern grid-scale energy storage systems, which are currently being explored with lithium-ion batteries (LIBs). However, this technology faces significant safety, social, and financial concerns. As an alternative chemistry, aqueous zinc-ion batteries (ZIBs) show much promise for grid-scale energy storage with their safe, inexpensive design. Major bottlenecks of ZIB performance include their limited practical specific capacity, and low capacity retention. Organic cathodes, specifically the use of redox-active quinone molecules, are an upcoming contender for customizable and simple ZIB cathode design that can be optimized for good performance. However, these cathodes are often plagued by capacity fade caused by quinone dissolution and inactivation. Grafting these quinone molecules to the supporting conductive carbon substrate via covalent bonding had been previously explored in LIB and supercapacitor electrode design as an effective way to mitigate capacity fade. In this work, the development of aqueous ZIB cathodes with 9,10-phenanthrenequinone (PQ) molecules grafted to carbon black substrates was done via a facile *in-situ* generated diazonium salt reaction synthesis technique. Electrochemical and material analysis confirmed the presence of covalent grafting. This grafting modification was compared to the standard cathode design of adsorbing the quinones on carbon substrates like Ketjenblack (KB) and Vulcan Black (VB). Battery cycling tests were performed and the grafted PQ-KB cells achieved a discharge capacity of

99 mAh g^{-1} after 1000 charge-discharge cycles with accelerated testing at a charge/discharge rate of 200 mA g^{-1} and 10 mA g^{-1}. These cells maintained 67% of their initial capacity compared to the 55% for the adsorbed PQ on KB cells. This approach highlights the promise of grafting organic material as a technique to support organic cathodes for next-generation ZIB design.

Acknowledgments

I would first and foremost like to thank Dr. Drew Higgins for supporting me in my undergraduate and graduate career in his lab. I am especially grateful for the opportunities he gave me including supporting me throughout this project.

Along with Drew, I would like to thank Dr. Stuart Linley, and Dr. Brian Adams for being members of my M.A.Sc. defence examination committee. I also would like to especially acknowledge Brian for all his support in this project and thank him for all the help he has provided me. Additionally, I would like to thank the other members at Salient Energy including Dr. Wendy Tran, and members of the McMaster zinc-ion battery team including Dr. Gillain Goward, her lab team, and Dr. Oleg Rubel.

I am very grateful to be on the zinc-ion battery team in Dr. Higgins's lab alongside my amazing colleagues: Alejandra Ibarra Espinoza, Storm Gourley, and Caio Miranda Miliante. I would not have been able to do any of this without their support. Additionally, I would like to thank Navid Noor, Arjun Rego, Hyejin Lee, and Erin Herzstein for their past support of my work in the lab and for helping me excel in energy storage research.

None of this could have been possible without the support of my family including my parents Laura and Stephen Baker, as well as Holly Baker, Gillian Baker, and Chris Burley. I would also like to extend gratitude to my girlfriend and fellow M.A.Sc. student Hannah Mann. Finally, this work was funded and supported by the Chemical Engineering department at McMaster University, NSERC, and Salient Energy Inc.

Table of Contents

Lay Abstract iii

Abstract iv

Acknowledgments vi

List of Figures x

List of Tables xiv

List of Abbreviations and Symbols xv

Declaration of Academic Achievement xviii

1. Introduction 1

1.1 Energy Storage Background 1

1.2 Battery Fundamentals 5

1.3 Aqueous Zinc-Ion Batteries 7

1.3.1 Inorganic ZIB Cathodes 8

1.3.2 Organic ZIB Cathodes 9

1.4 Covalent Grafting 11

1.5 Research Motivation 14

1.6 Research Objectives 15

2. Experimental Methodology 17

2.1 Battery Cycling 17

2.2 Rate Capability Testing (RCT) 19

2.3 Galvanostatic Intermittent Titration Technique (GITT) 20

2.4 Cyclic Voltammetry (CV) 21

2.5 Electrochemical Impedance Spectroscopy (EIS) 24

2.6 Fourier Transform Infrared (FTIR) Spectroscopy 28

2.7 Thermogravimetric Analysis (TGA) 29

3. Project Investigation 30

3.1. Abstract 31

3.2. Introduction 32

3.3. Experimental Methods 37

3.3.1. Materials 37

3.3.2. Cathode Synthesis Procedure 37

3.3.3. Cathode Synthesis and ZIB Assembly 41

3.3.4. Electrochemical testing 42

3.3.5. Material Characterization 43

3.4. Results and Discussion 44

3.5. Conclusion 64

4. Conclusions and Future Work 65

5. References.....68

Appendix: Manuscript Supporting Information.....78

List of Figures

Figure 1. Electrical energy production in Ontario by generation source in September 2023, provided by Ontario's Independent Electricity System Operator [3]. 2

Figure 2. Installed global energy storage system breakdown by storage technology [7]. ..3

Figure 3. Ragone plot of electrochemical energy storage technologies with approximate discharge times, reproduced from [4]. 4

Figure 4. Diazonium salt grafting mechanisms; (a) radical generation, (b) monolayer grafting, (c) and (d) multilayer grafting, reproduced from [33].....12

Figure 5. Profile of a typical battery or faradaic electrochemical device with (a) applied current, (b) charge-discharge curves, (c) CV curve, reproduced from [39].....18

Figure 6. Typical CV with IUPAC convention labeling, reproduced from [43]. 22

Figure 7. (a), (b), (d), (e), (g), (h) CV curves and (c), (f), (i) discharge curves of typical electrochemical devices depending on active material mechanism, reproduced from [45]. 23

Figure 8. Examples of a simple a) Nyquist plot and b) Bode plot. 25

Figure 9. Equivalent circuit and Nyquist plot of a Randles circuit, adapted from [46]. ...27

Figure 10. Schematic of grafted organic cathode ZIB battery operating in grid scale energy storage with inset showing zinc coordination with quinone molecules covalently grafted to a carbon support.....36

Figure 11. Synthesis procedure for forming 9,10-phenanthrenequinone precursors and grafting them to carbon substrate.....40

Figure 12. FTIR spectra of pristine PQ and cathode materials (quinone, KB, PTFE) with characteristic peaks highlighted in blue for a) Pristine PQ (C=O stretch), b) PQ-NH_2 (primary NH_2 stretching and bending) , c) PQ-NO_2 (NO_2 stretching), d) chemically grafted PQ-KB (C=O stretch). 46

Figure 13. TGA curve of a) PQ, cathode materials b) adsorbed PQ to KB and c) chemically grafted PQ-KB, along with d) KB, ramped to 1000 °C at a rate of 10 °C min^{-1}. 48

Figure 14. SEM images of a) pristine adsorbed PQ on KB cathode, b) pristine chemically grafted PQ-KB cathode, c) chemically grafted PQ-KB cathode after the first charge d) chemically grafted PQ-KB cathode after the second discharge.....49

Figure 15. CV curves of cathode materials (PQ:CB:PTFE) at 1 mV s^{-1} for chemically grafted PQ 4:5:1, and adsorbed PQ on the carbon black substrate with 6:3:1 and 4:5:1 material ratios for a) KB and b) VB.....50

Figure 16. Linear fit of relations derived from CV between scan rate (ν) and peak oxidation current (I_P) for b-value analysis for chemically grafted PQ 4:5:1 (PQ:CB:PTFE), and adsorbed PQ on the carbon black substrate with 6:3:1 and 4:5:1 material ratios for a) KB and b) VB.....51

Figure 17. EIS Nyquist plots of chemically grafted PQ 4:5:1 (PQ:CB:PTFE), and adsorbed PQ on the carbon black substrate with 6:3:1 and 4:5:1 material ratios for a) KB and b) VB at OCP. 53

Figure 18. Rate capability testing with discharge capacities of a) KB supported cathodes and b) VB supported cathodes. 54

Figure 19. Accelerated cycling testing of cells with a RPT current density of 10 mA g^{-1} performed on KB supported cells (top) and VB supported cells (bottom) with a) & c) showing discharge capacity, b) & d) showing discharge capacity retention. Error represents standard deviation of duplicate tests. 56

Figure 20. Charge and discharge curves for ZIBs with a) chemically grafted PQ-KB cathode, b) adsorbed PQ on KB cathode, c) chemically grafted PQ-VB cathode, and d) adsorbed PQ on VB cathode 6:3:1 (PQ:CB:PTFE). The curves for the sample adsorbed PQ on VB cathode 4:5:1 are seen in **Figure S4**. 58

Figure 21. Slow cycling testing of cells with a current density of 10 mA g^{-1} performed on KB supported cells (top) and VB supported cells (bottom) with a) & c) showing discharge capacity, b) & d) showing discharge capacity retention. Error represents standard deviation of duplicate tests, triplicate test for grafted PQ-KB. 60

Figure 22. Galvanostatic Intermittent Titration Technique (GITT) profiles for a) chemically grafted PQ-KB 4:5:1 (PQ:CB:PTFE), b) chemically grafted PQ-VB 4:5:1, c) adsorbed PQ on KB 6:3:1, d) adsorbed PQ on VB 6:3:1, e) adsorbed PQ on KB 4:5:1, and f) adsorbed PQ on VB 4:5:1 63

Figure S1. a) FTIR spectrogram and b) mass spectrogram of residue recovered from washing grafted PQ-KB material. 81

Figure S2. CV curves of crude cathode material (quinone, Vulcan black, PTFE) at 10 mV s^{-1} before solvent washing (red) and after washing (blue) for a) chemically grafted PQ, b) adsorbed PQ, e) adsorbed PQ-NH_2. 81

Figure S3. Equivalent model circuit for fitting EIS data. R1 represents the solution resistance, Q2 and R2 are the thin film electrolyte-electrode interface constant phase element and resistor respectively, R3 represents the R_{CT}, and Q3 and W3 are the cathode constant phase element and Warburg element respectively. 82

Figure S4. Charge and discharge curves for ZIBs with adsorbed PQ on VB cathode (4:5:1).....82

Figure S5. FTIR spectra of purified chemicals with characteristic peaks highlighted for a) PTFE, b) PQ-NH_2 (primary NH_2 stretching and bending), c) PQ-NO_2 (NO_2 stretching), d) VB. 83

Figure S6. Diagram of capacity retention relating to PQ stabilization from grafted PQ 4:5:1 (PQ:CB:PTFE) and adsorbed PQ 4:5:1 with porous KB vs. non-porous VB carbon supports. 84

List of Tables

Table 1. Accelerated cycling performance metrics for adsorbed and grafted cathodes (PQ:CB:PTFE). Error represents standard deviation of duplicate tests. 55

Table 2. Slow cycling performance metrics for adsorbed and grafted cathodes (PQ:CB:PTFE). Error represents standard deviation of duplicate tests, triplicate test for grafted PQ-KB. 59

Table S1. Six tested cathode material samples and their respective PQ loadings..... 80

List of Abbreviations and Symbols

a	*b*-value Equation Coefficient
AC	Alternating Current
ATR	Attenuated Total Reflectance
b	*b*-value
C	Capacitor
C_{dl}	Double Layer Capacitance
CE	Coulombic Efficiency
CV	Cyclic Voltammetry
D	Diffusion Coefficient
DOE	Design of Experiments
ΔE_S	GITT Voltage Change between Steady States
ΔE_τ	GITT Current Pulse Voltage Change
EDLC	Electrochemical Double Layer Capacitance
EIS	Electrochemical Impedance Spectroscopy
FTIR	Fourier Transform Infrared Spectroscopy
GITT	Galvanostatic Intermittent Titration Technique
I_P	CV Peak Current
IUPAC	International Union of Pure and Applied Chemistry
L	Inductor
LIB	Lithium-Ion Battery

LSV	Linear Slope Voltammetry
NMC	Nickle Metal Cobalt Oxide
M_B	GITT Active Material Molar Mass
m_B	GITT Active Material Mass
MMO	Mixed Metal Oxide
OCP	Open Circuit Potential
PANI	Polyaniline
Q	Constant Phase Element
R	Resistor
R_{CT}	Charge Transfer Resistance
R_S	Solution Resistance
R_U	Uncompensated Resistance
RCT	Rate Capability Testing
RPT	Reference Performance Test
RTE	Round-trip Efficiency
S	GITT Cathode Geometric Surface Area
SEM	Scanning Electron Microscopy
τ	GITT Current Pulse Time
TGA	Thermogravimetric Analysis
ν	CV Scan Rate
V_M	GITT Active Material Molar Volume
W	Warburg Element

Z’	Real Impedance
Z’’	Imaginary Impedance
Z_W	Warburg Impedance
ZIB	Zinc-Ion Battery

Declaration of Academic Achievement

I, Thomas J. Baker, declare that this thesis titled, “Development of Stabilized Organic Cathodes via Grafting Redox-active Molecules to Carbon in Aqueous Zinc-ion Batteries for Energy Storage Systems” and the work presented in it are my own.

1. Introduction

1.1 Energy Storage Background

It is well understood that climate change is caused by greenhouse gas emissions released by human activity. The second largest source of greenhouse gas emissions in the United States in 2022 was from electrical power generation (24.8 % of all emissions) [1]. This is mainly due to the burning of non-renewable fossil fuels in conventional power generation. However, in a recent push to lower greenhouse gas emissions, countries have been adopting renewable power sources to supply electricity for their national grids. Renewables now account for over 25% of the amount of electricity production globally [2]. Nevertheless, there is one fundamental challenge facing renewable energy production and that is their intrinsic intermittency. For example, both wind and solar power generation are becoming increasingly incorporated as sources of electricity generation for greener power grids. However, both sources are highly weather dependent and will severely lack production frequently depending on the time of day and local conditions. As seen in **Figure 1** electricity production in Ontario in September 2023, had significant contributions of renewable generation, but it ranged notably over the days.

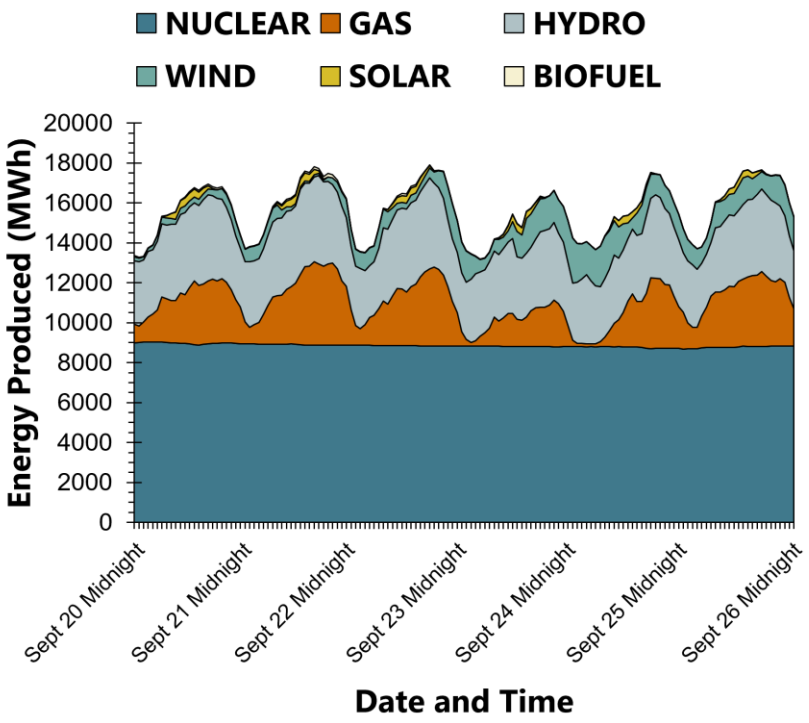

Figure 1. Electrical energy production in Ontario by generation source in September 2023, provided by Ontario's Independent Electricity System Operator [3].

To make up for the temporary lack of electricity supply of renewable energies, power generation by natural gas combustion increased. This overall demonstrates that despite the incorporation of renewable sources, the grid is still dependent on fossil fuel combustion to pick up the slack caused by the intermittent nature of renewables. However, this intermittency problem can be addressed with proper grid-scale energy storage. Grid-scale energy storage is the application of large, usually stationary, energy storage systems for the main purpose of storing energy produced by renewables (or other sources) when production is higher than demand so that the stored energy can be used later when production decreases below the demand [4], [5]. Electrical energy storage can be provided

by many different technologies. As seen in **Figure 2** majority of installed global energy storage is currently gravity-driven pumped hydro storage. However, this technology is geographically limited and dependent on large bodies of water. With the recent surge in grid-scale energy storage demand, alternatives that can be easily adapted to different environments and have scaled-up potential, like electrochemical energy storage, have been making up the majority of the newly installed storage capacity [6].

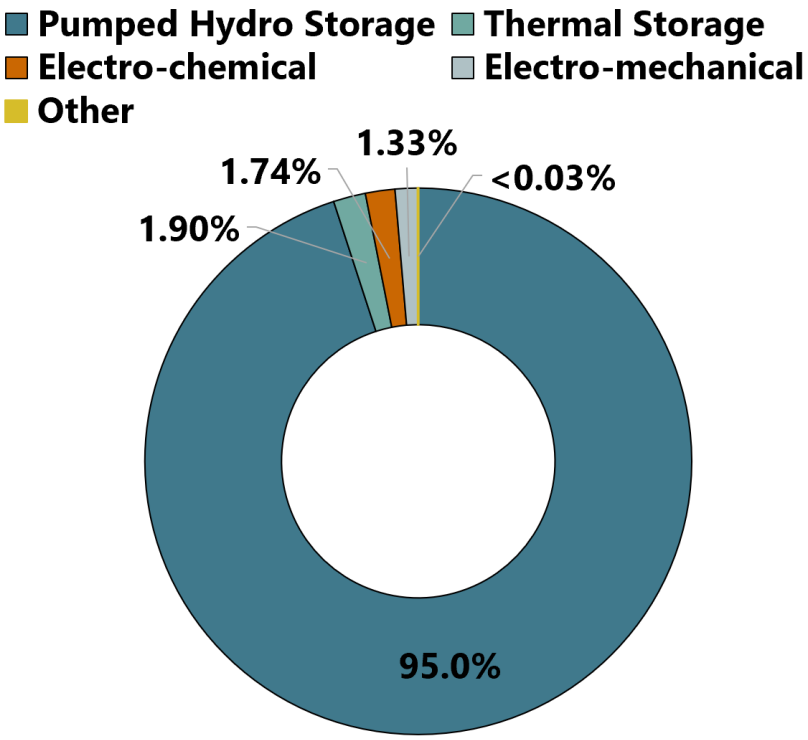

Figure 2. Installed global energy storage system breakdown by storage technology [7].

Batteries adequately fill the niche for grid-scale energy storage. As seen in **Figure 3** various battery chemistries would be suitable for grid-scale energy storage as they do not require fast charging/discharging conditions since the time range for grid-energy storage is

typically around 4 – 6 hours [6]. Thus, batteries' high energy density and modular design make them ideal for new grid-scale energy storage infrastructure. [4], [6].

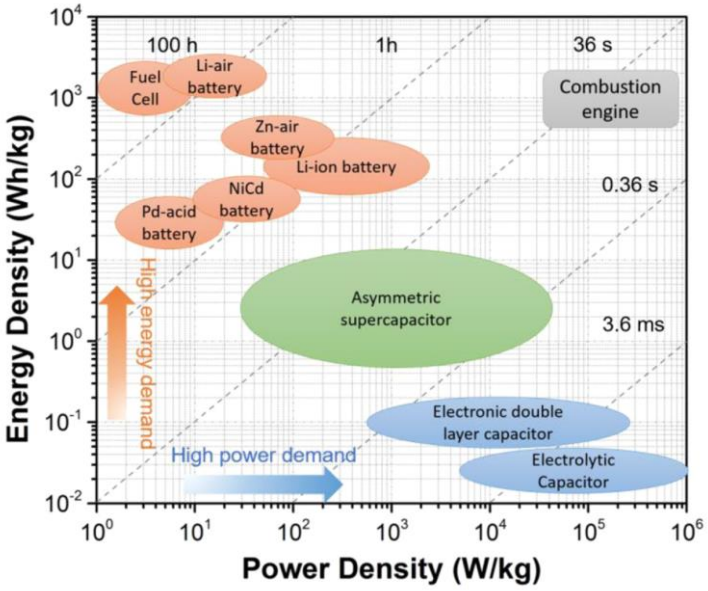

Figure 3. Ragone plot of electrochemical energy storage technologies with approximate discharge times, reproduced from [4].

1.2 Battery Fundamentals

Batteries are electrochemical devices that store charge (and thus energy) mainly via faradaic reactions, which are fast and reversible reactions that occur with the active material in the batteries' electrodes [4]. The faradaic reactions are driven by an electrochemical gradient caused by a potential difference between the two electrodes of the battery: the anode and cathode. These electrodes are spatially separated within the battery via a separator which is electrically insulating, but the electrodes are ionically connected via an electrolyte. When the battery is charging the active material on the cathode is oxidized and the anode is reduced, the opposite is true during discharge. Batteries applied in grid-scale storage are secondary or rechargeable batteries meaning that they are subjected to many charge and discharge cycles over their lifetime. Although rechargeable batteries traditionally consisted of lead-acid, nickel cadmium, and nickel–metal hydride chemistries to store charge, these battery types have largely been replaced with lithium-ion batteries (LIBs) for large energy storage applications [6], [8].

LIBs have anodes composed of graphitic carbon which allows for the intercalation of Li^+ ions. During discharge, these ions migrate to the cathode through an organic electrolyte. These ions will intercalate with the cathodic material which is often selected to be $LiCoO_2$, $LiFePO_4$, or Nickle Metal Cobalt Oxide (NMC) [8], [9]. LIBs are particularly attractive choices for energy storage as their chemistry allows for high nominal cell voltages (3 V – 4 V) and high theoretical capacity, which translates to a high energy density [8]. The high gravimetric and volumetric energy density in LIB is reinforced by the intrinsic

lightweight nature of lithium, making these batteries excellent candidates for portable energy storage applications like personal electronic devices and electric cars [8]. However, there are some significant concerns with LIBs. Among them is the exothermic instability of lithium in contact with air or water. Additionally, the organic electrolytes employed in most LIBs are very flammable. Thus, there have been many reported cases of LIB cell failure leading to thermal runaway, in which the batteries catch fire and pose a significant safety risk [8], [9]. The extraction of the materials necessary for LIBs has several environmental and social consequences. The extraction of lithium carbonate (precursor of the cathode material) requires enormous amounts of water, and the rarity, difficult extraction, and processing of lithium drives up its cost. It was estimated that in 2022, the market price of lithium carbonate was $78,009 USD per tonne, or about 35 times more expensive than manganese (another metal used in cathode development) [10]. This cost is only expected to rise as demand for LIBs outpaces the global supply of lithium [6]. Finally, the mining of carcinogenic cobalt for LIB cathodes is unethically sourced from the Democratic Republic of the Congo where it causes social and environmental distress [11]. These intrinsic problems with LIBs spurred researchers to investigate the feasibility of alternative battery chemistries like sodium-ion batteries, and zinc-ion batteries.

1.3 Aqueous Zinc-Ion Batteries

As a possible replacement to LIB, especially for grid-scale energy storage, zinc-ion batteries (ZIBs) have several intrinsic benefits worth noting. An aqueous ZIB is a battery composed of a metallic zinc anode and an aqueous electrolyte of a zinc salt such as $ZnSO_4$ [6]. Zinc metal has high theoretical capacities of 820 mAh g^{-1} and produces divalent Zn^{2+} ions that transverse the cell carrying twice the charge of a Li^+ ion, giving ZIB the potential to have high performance [6], [12]. The aqueous electrolyte also means these batteries have no risk of thermal runaway and catching fire [6], [12]. Additionally, ZIBs inherently have several characteristics that would make them cheaper to manufacture than LIBs, like for example, the relatively inexpensive zinc metal. Furthermore, unlike lithium, zinc is air and water stable, meaning all the costly manufacturing and transportation modifications necessary to maintain a moisture and air free environment during LIB cell assembly are not necessary in ZIB assembly [6]. The use of zinc and an aqueous electrolyte also means cell disassembly and recycling as an end-of-life option for ZIBs is much more practical and easier to undertake using conventional technologies, adding to the sustainability nature of these energy storage devices [6].

Fundamentally, zinc metal works as an electrode material in a battery due to the fact that it employs a mechanism where the Zn^{2+} ions strip and plate upon the zinc anode when the cell is cycling. Like in LIBs the ions migrate through the electrolyte to the cathode to interact with it and store charge. However, many different cathodic chemistries are being explored and each has a unique way of storing charge. Since, the biggest bottleneck noted

in ZIBs is the lack of capacity and low capacity retention of many cathodic materials used in them, different cathode chemistries are being explored.

1.3.1 Inorganic ZIB Cathodes

The most conventional cathode design for current ZIB could be described broadly as utilizing inorganic active material to store charge. Specifically, these cathodes utilize materials like mixed metal oxides (MMOs) or Prussian blue analogues (PBAs). These materials generally utilize an intercalation mechanism with the incoming Zn^{2+} ions during discharge to store charge. For example, many MMO cathodes made of vanadium oxide ($Zn_{0.25}V_2O_5 \cdot nH_2O$), manganese dioxide ($MnO_2$), and cobalt oxide were able to achieve high cathodic/cell capacities and capacity retentions utilizing an intercalation mechanism in a ZIB [5], [13], [14]. Specifically, MnO_2 has been sought after as a standard ZIB cathodic material as it tends to have a high discharge capacity(>250 mAh g^{-1}) [5]. However, MnO_2 suffers from significant capacity fade/loss as the battery cycles which is caused by Mn^{2+} dissolution into the electrolyte due to the Jahn-Teller effect [15]. This dissolution is induced during discharge via a disproportionation reaction and causes the subsequent reformation of Zn-MnO_2 analogues on the cathode during charge that prevents the cathode from maintaining the same intrinsic capacity [6], [14]. Additionally, as it was previously mentioned cobalt is an unfavourable material to work with, and vanadium cathodes also face dissolution capacity loss undergoing slow discharge, which would be expected for grid-scale applications [15]. Finally, inorganic cathodes are mineral dependent requiring

extensive procurement, extraction, and processing even before application in a cathodic material [12].

1.3.2 Organic ZIB Cathodes

As an alternative to inorganic cathodes, recent developments have been made in applying redox-active organic molecules for cathode materials in ZIBs. These molecules range greatly, but in a ZIB cathode, they utilize surface redox reactions to store charge through Zn^{2+} coordination and proton interactions. They are often accompanied by a conductive carbon support in the cathode. They are particularly interesting for ZIB applications as they have flexible and tunable structures that can be optimized for best performance, in addition to the fact that their synthetic nature lacks the mineral limitations of inorganic materials and can be made sustainable with the correct manufacturing adaptations. There are many different types of organic molecules used in ZIB cathodes. For example, polymers like conductive polyaniline (PANI) have been well documented to store charge well through redox reactions when incorporated with a carbon substrate [12], [16]. Small organic compounds that are redox-active have also been extensively applied in ZIBs. In general, the compounds contain aromatic carbon backbones with redox-active motifs based on heteroatom incorporation such as sulfur, cyan, imine, or carbonyl motifs [17]. Specifically, a class of redox-active molecules known as quinones has had recent success as an active material in electrochemical energy storage devices. Quinones are organic molecules that contain two or more redox-active carbonyl groups supported by an aromatic

backbone [18]. The redox activity of the carbonyl groups along with the π-π interactions of the aromatic rings (which yields effective charge transfer) allow for good electrochemical performance in a wide range of devices. For example, quinones have been studied for use in flow batteries, pseudocapacitors, dye-sensitized solar cells, and artificial photosynthesis among others [18].

In energy storage, there has been a lot of interesting work on incorporating different quinones into electrodes for supercapacitor [19]–[22] and LIB applications [23]–[25]. Recently they have also shown much promise in aqueous ZIBs. From smaller molecules like naphthoquinone on carbon nanotubes to large molecules like phenanthrenequinone triangles on acetylene black, many different quinone arrangements have been tested for ZIB cathodes [26], [27]. Despite often having reasonable initial capacities and relatively easy synthesis, quinones face one significant disadvantage: capacity fade. Although the degradation mechanism(s) is a subject of current research, some studies have shown that the dissolution of quinone can occur during battery cycling and cause capacity fade [26]. More recently this mechanism has been thought to be a phase evolution caused by the temporary dissolution of quinones during discharge that then form electrochemically inactive crystal structures through Ostwald ripening [5], [28]. Over time with the loss of quinone active material, the capacity of the cathode is lost, and this instability is one of the main reasons why organic cathode design faces challenges to becoming the cathode active material of choice.

1.4 Covalent Grafting

Covalent functionalization of carbon materials is a technique to reduce dissociation and structural change of active materials that would normally only be stabilized on carbon materials through non-covalent interactions, like π-π interactions [29]. This process, also known as grafting, can be applied to many organic molecules and polymers. In an attempt to maintain the redox activity of quinones, grafting these molecules to carbon has recently become of great interest to researchers. There are different ways to graft organics to carbon depending on the molecule and carbon substrate being used. Redox-active molecules can be grafted through amidation reactions, ring-opening reactions, diazonium salt reactions, cyclization reactions, esterification reactions, or more [29]. However, diazonium salt reactions have a particular advantage for grafting as they form grafted molecules that bond perpendicular to the plane of the carbon substrate they are on, which is useful for molecular accessibility in redox reactions with the electrolyte. This can prevent graphene sheets from aggregating when reduced graphene oxide is functionalized [29]. It also allows grafting to easily occur on non-planar carbon substrates like carbon nanotubes and carbon black.

Diazonium salt reactions refer to the reduction of a molecule with a diazonium functional group attached ($N\equiv N^+–R$) where R represents an aromatic ring. These functional groups are inherently unstable and will cleave the diazonium group to form nitrogen gas (which bubbles off) and an aryl radical [30]. The radical will then target sp^2 hybridized carbons such as the ones found on a carbon substrate and form a covalent bond grafting the molecule (see **Figure 4**) [29], [30]. This can also result in the radical molecule targeting

other grafted molecules which leads to the formation of oligomer chains on the substrate surface forming a multilayer as opposed to a monolayer of grafted monomers [30]. The covalent bonds formed can be direct C – C bonds or bonds through an azo linkage if the radical mechanism happens to react with a diazonium salt (see **Figure 4** and **Figure 11** to see the different bonding results) [30]. Additionally, this method can also be adapted to allow the grafting of molecules to other substrates. For example, grafting to metal surfaces has been reported with iron, palladium, copper, gold, titanium, and even zinc [30], [31]. It can even allow grafting to silicon and many polymers [30], [32].

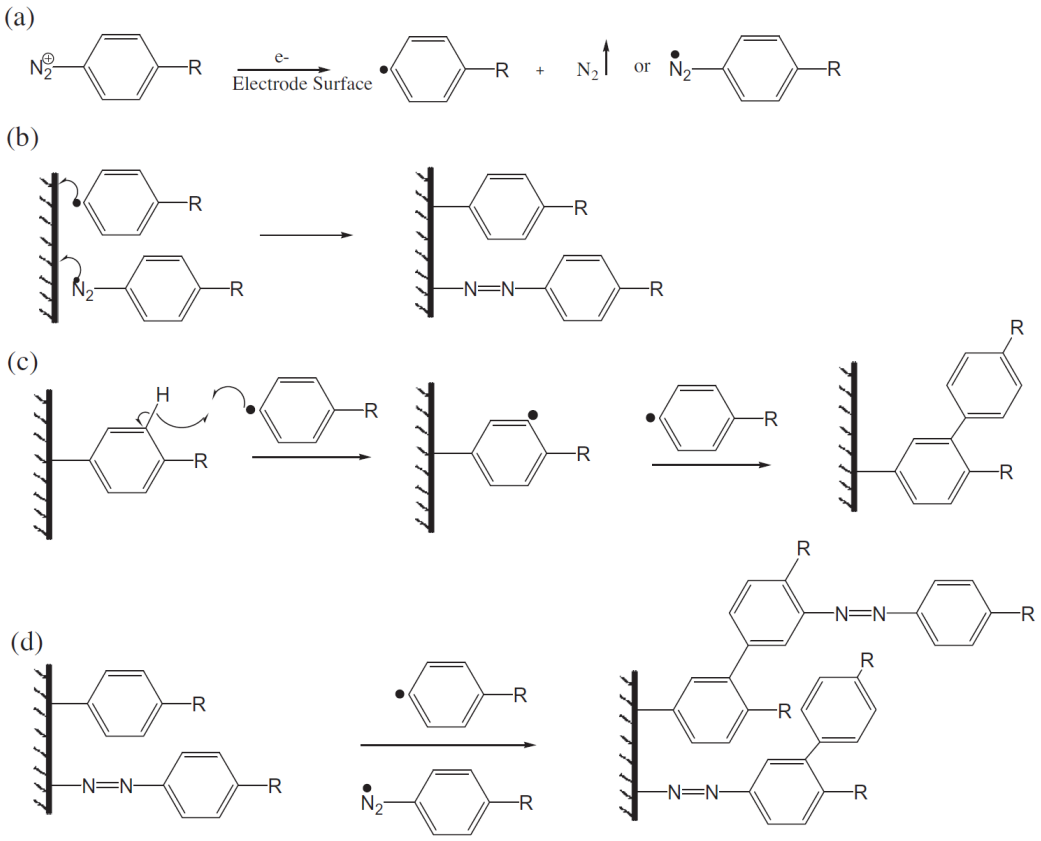

Figure 4. Diazonium salt grafting mechanisms; (a) radical generation, (b) monolayer grafting, (c) and (d) multilayer grafting, reproduced from [33].

As mentioned before the grafting process can occur through a spontaneous chemical reaction between the substrate and the diazonium salt. Although the salt can be prepared beforehand and then added to the substrate in solution, this is not typically done by researchers exploring grafting for energy storage. This is because the diazonium salt is highly unstable and, diazonium salts like diazonium chloride violently explode when isolated [34]. Instead, researchers generally elect to form the diazonium salt *in situ* and allow it to subsequently react and graft, eliminating the aforementioned safety risk. This can be done by converting an amino group (on an aryl backbone like a quinone) to a diazonium salt in solution via tert-butyl nitrite in an acetonitrile solvent or sodium nitrite in a sulfuric acid solution for example [35], [36]. The carbon substrate would also be present in these solutions allowing for immediate reduction of the diazonium salt after it is formed. Similarly grafting can be employed electrochemically by setting the carbon substrate as an electrode. The diazonium salts will reduce and graft to the electrode surface when the potential is lowered on the electrode [30]. This can give one control over the reaction and can be used in the presence of grafting inhibitors to control the formation of the grafted layer into a monolayer or a multilayer [37]. Since diazonium salt grafting only requires a diazonium group attached to an aromatic ring, this grafting process can be applied to all quinones and many other organic compounds. The use of diazonium grafting to stabilize electrodes in other electrochemical systems has been done before. Mainly it has had much success at stabilizing quinones on supercapacitor electrodes and stabilizing quinones and aryl organics on LIB cathodes and anodes [33], [35], [36], [38].

1.5 Research Motivation

Even though the application of diazonium salts to graft quinones to carbon substrates has been used to successfully stabilize organic cathodes in LIBs and supercapacitors, no study has looked into using this technique for organic cathodes in ZIBs. Since dislocation of adsorbed quinones during cycling is currently believed to contribute to capacity fade, grafting and thus fixing the quinone to the carbon substrate should improve capacity retention of ZIBs with quinone-based cathodes. The project described herein is aimed to prove the previous statement. In general, there is a lot of flexibility to investigate this technique. ZIBs have a reputation of being a less expensive, safer, and more sustainable alternative to conventional LIBs. The use of organic cathodes backs up this idea. Diazonium grafting can be seen as an extension of that idea: a simple modification that improves the efficacy of organic cathodes in ZIBs while minimizing extra synthesis complexity. The concept of grafting quinones to carbon substrates for ZIB cathodes inherently has a lot of possibilities regarding synthesis conditions and materials use, so this work will highlight this technique as an initial investigation to prove its utility in ZIB development. With results presented and discussed using standard experimental methodology for ZIB design, this thesis aims to set up grafting to stabilize quinones in ZIB cathodes as an initial step that can be built upon in future studies.

1.6 Research Objectives

1) Produce a grafted 9,10-phenanthrenequinone (PQ) cathode for ZIBs that allows a discharge capacity retention above 70% and a discharge capacity above 100 mAh g^{-1} to be achieved for 1000 cycles at an accelerated testing of 200 mA g^{-1} with 10 mA g^{-1} reference performance tests.
    - The main desire of this project is to show how grafting quinones to carbon substrates should stabilize electrodes as predicted in literature.
    - Thus, it is necessary to demonstrate the utility of this technique by highlighting its performance under accelerated testing to a standard that surpasses adsorbed PQ expectations.
2) Validate the existence of a grafted quinone – carbon modification through electrochemical impedance spectroscopy (EIS), Fourier-transform infrared spectroscopy (FTIR), and thermogravimetric analysis (TGA).
    - In order to be confident that any performance improvements are a result of grafting, grafting must be proven by techniques highlight in the literature.
    - Although one test is likely insufficient to prove grafting, by utilizing multiple different tests general trends that are expected to be seen by grafted materials can be discerned.
3) Identify ideal carbon substrate properties (e.g. surface area, porosity) and active material to carbon ratios for both grafted and adsorbed PQ with respect to PQ stabilization.

- It is important to investigate the stability and capacity effects that different carbon substrates have on adsorbed and grafted quinones, with different material ratios.
- It is desirable to use inexpensive and easy-to-acquire carbon substrates with respect to scale-up design so long as the performance effects of the carbon substrate are understood for future optimum cathode development.

2. Experimental Methodology

2.1 Battery Cycling

Also known as Galvanostatic Charge/Discharge (GCD) testing. This test focuses on measuring voltage changes over time with a controlled current/current density [39]. The direction of the current (current sign) controls whether the battery is charging or discharging. A voltage window is set up so the current will cause the voltage to change over time from one limit to the other and then the current is reversed to return to the original voltage limit, thus completing one cycle which contains a discharge and charge curve (see **Figure 5** b). This can be done using a potentiostat or a battery tester designed to cycle cells. There are different ways to display battery cycling data, one of the most common techniques is to plot the data as a charge and discharge curve. In this plot the x-axis represents capacity, and the y-axis represents cell voltage. The are two lines plotted for a cycle, one for the discharge and one for the charge. Capacity is often normalized by the active material mass (mAh g^{-1}) or electrode area (such as the electrode geometric area, mAh cm^{-2}), to allow for fair comparisons between cells [39]. The current can similarly be normalized for the same reasonings to compare experiments via a standard current density (mA g^{-1}). However, it is also common to run cells at what is known as a specific C-rate. For example, a C-rate of C/20 represents the amount of current needed to fully charge/discharge the battery in 20 hours [39]. Charge/discharge curves of batteries are noted for their plateaus where the change in cell voltage remains more constant as the capacity increases. This phenomenon represents the redox activity of the active material

and corresponds to the peaks in CV (see **Figure 5** c) [39]. While observing straight lines on a charge/discharge curve, forming an "X" pattern, represents electrochemical double layer capacitance (EDLC), an electrochemical response more predominant in supercapacitors than batteries [40].

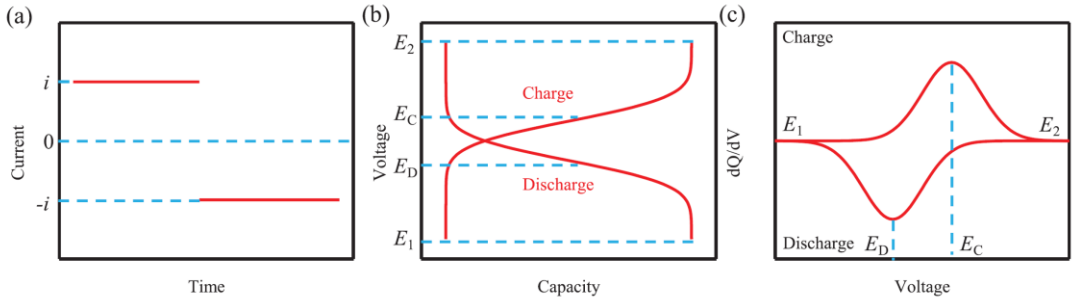

Figure 5. Profile of a typical battery or faradaic electrochemical device with (a) applied current, (b) charge-discharge curves, (c) CV curve, reproduced from [39].

Additionally, there are two efficiency metrics discerned from charge/discharge curves. First, there is the Coulombic Efficiency (CE) which is the ratio of discharge over charge capacity. This can be noted by comparing the maximum charge capacity of the charge and discharge curves [39]. Then there is the energy efficiency or Round-trip Efficiency (RTE). Similar to the CE, the RTE is the ratio of discharge over charge energy capacity.

2.2 Rate Capability Testing (RCT)

RCT is a modified battery cycling test that is used to highlight how the cell responds to different charge/discharge current rates by subjecting it to an increasing rate and observing how capacity changes at the higher currents (see **Figure 18**). The current can then be returned to the original value, and the capacity can be compared to the original capacity. In general, it is expected that the capacity of the cell decreases as the current increases due to aggravated polarization occurring in the cell [39]. A cell that does not lose much capacity as the current rate increases is generally desired as it has a more flexible design for charge/discharge times that will likely vary in real energy storage systems.

2.3 Galvanostatic Intermittent Titration Technique (GITT)

The Galvanostatic Intermittent Titration Technique (GITT) is an electrochemical method for determining the chemical diffusion coefficient of ions in the electrode material in battery cells [41]. This technique was first proposed by Weppner and Huggins in 1977 [42]. Specifically, this would be the diffusion coefficient of Zn^{2+} ions and other charge carriers into and through the cathode in ZIBs. The diffusion coefficient is used as a metric to evaluate how the formulation and structure of the electrode materials affect Zn^{2+} movement and accessibility in the cell. In general, the process involves applying a current pulse to the cell which results in a voltage drop or increase. The cell is then allowed to rest where ion diffusion gives way to a stable cell voltage. This process repeats until a full charge or discharge potential is obtained [41]. Derived from Fick's second law, and simplified for a small applied current time, the diffusion coefficient can be determined from Equation 2 [41]. Given the specificity of the material data needed to calculate the diffusion coefficient and the batch-to-batch variation in electrode design, it is important to point out that the diffusion coefficient calculated is an approximate value. The choice of calculation assumptions can have a great effect on the final diffusion coefficient answer [41]. This is especially true in the evolving field of ZIBs.

2.4 Cyclic Voltammetry (CV)

Cyclic Voltammetry is a very important technique commonly used in electrochemistry research that allows observation of the electrochemical activity of an electrode at different potentials. CV works by subjecting an electrode of interest to a potential compared to a standard reference electrode. This can be done in a three-electrode cell to investigate a material of interest on the working electrode, measuring the potential with a reference electrode (e.g. standard hydrogen electrode, Ag/AgCl electrode), and completing the circuit with current flow through a counter electrode [43]. In the case of ZIBs, CVs can also be set up in a two-electrode cell where the zinc metal anode acts as both the reference electrode and the counter electrode. The cell would be controlled through the use of a potentiostat/ galvanostat. This technique involves sweeping the potential experienced at the working electrode across a potential window at a particular scan rate ($mV\ s^{-1}$). Each moment the potential will elicit a current response. The behaviour of the current response at particular potentials depends on the electrode material. After sweeping from one bound of the potential window to the other, the next sweep will be in the reverse direction. Whereas linear sweep voltammetry (LSV) will only occur in one direction, CV will sweep to return to the original potential thus allowing one to see the electrochemical oxidation and reduction of the material. By IUPAC convention the oxidation sweep corresponds to positive currents and is plotted above the reduction sweep in voltammograms (**Figure 6**) [43].

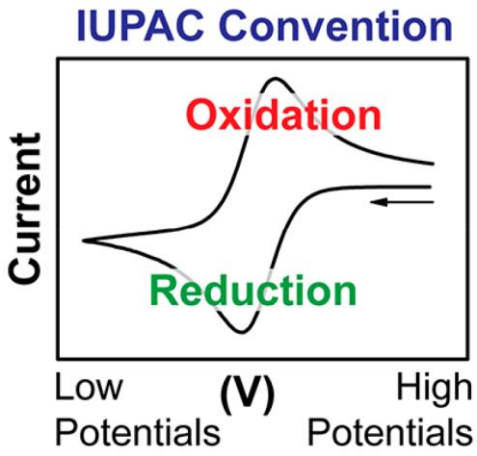

Figure 6. Typical CV with IUPAC convention labeling, reproduced from [43].

The power of CV as a technique comes from the fact that the shape of the CV curve explains the performance of the electrode/cell. EDLC, as expected in supercapacitors, is observed to be a rectangular shape in CV with constant currents for the oxidation and reduction sweeps. However, redox-active materials have distinct peaks at the potentials where the reduction or oxidation reaction is expected to occur [43]. The shape and area of the CV curves correspond with the charge/discharge curve shape. Notably, the peaks of a CV curve generally line up with the plateaus on a charge/discharge curve (**Figure 5**). Thus, the electrochemical activity of an electrode can be characterized into specific subcategories with corresponding CV and charge/discharge curves as seen in **Figure 7**. In theory, the reduction and oxidation peaks of an electrochemically reversible species should line up with each other on a CV curve. However, kinetic limitations in real systems result in slight overpotentials that give rise to peak shifts (more potential needed to drive the same current response) [43]. So, peak shift is expected to increase as the scan rate increases. This is

because at high scans, not enough time is allotted for an electrochemical reaction (that produces current) without large potentials pushing the reaction. The relationship between scan rate and peak current can be modeled with Equation 1. This model and the deduction of the *b*-value in Equation 1 is known as b-value analysis. The value of *b* can be solved through regression and corresponds to a description of the electrochemical behaviour of the active material. If $b = 0.5$ the electrochemical process is diffusion controlled, if $b = 1$ the process is surface controlled by redox reactions and/or capacitance, and if *b* is between 0.5 and 1, the process is controlled by a combination of both mechanisms [40], [44].

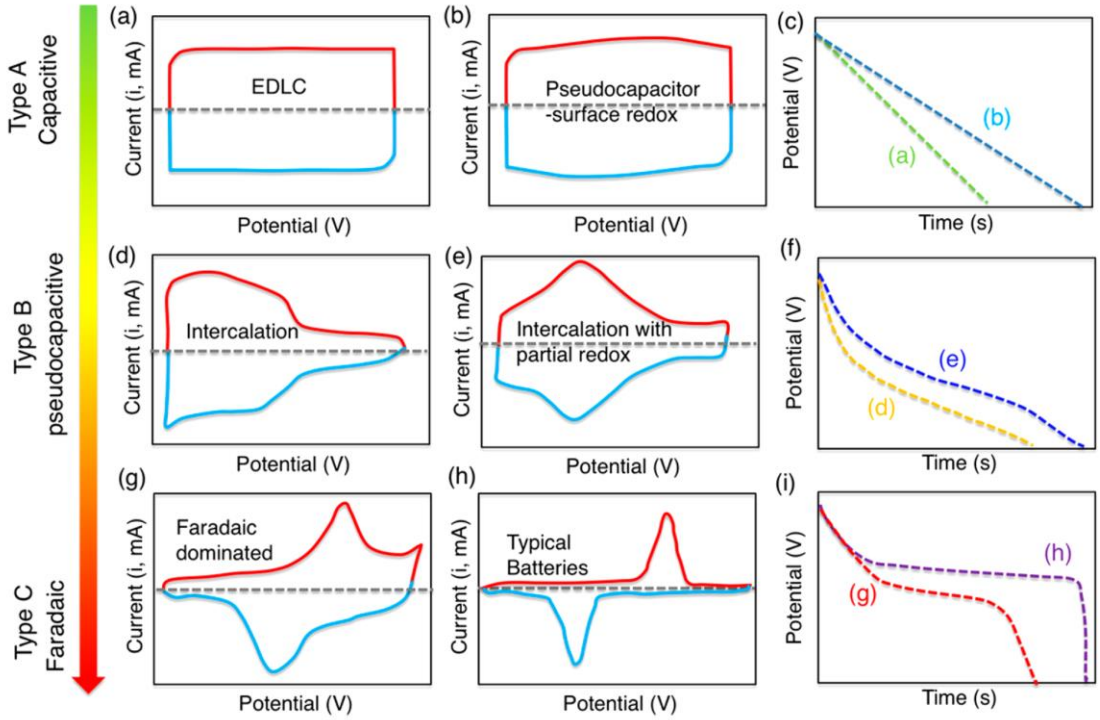

Figure 7. (a), (b), (d), (e), (g), (h) CV curves and (c), (f), (i) discharge curves of typical electrochemical devices depending on active material mechanism, reproduced from [45].

2.5 Electrochemical Impedance Spectroscopy (EIS)

EIS is an advanced electrochemical characterization test that is used to give mechanistic insight into electrochemical systems by utilizing alternative current (AC) to modulate the electrode potential at various frequencies and record the response of the system. Physically EIS can be set up the same as CV with a three or two-electrode cell, operating on a potentiostat/galvanostat. EIS looks at comparing the output AC signal to the input AC signal as the basis for deducing the system mechanism. Generally, this can be seen as comparing the input oscillating voltage to the output oscillating current with a phase shift between the signals. The transfer function that compares the input voltage to the output current is analogous to Ohm's law (in which voltage and current are related to each other through resistance) and is known as impedance [46]. Similar to resistance, impedance is measured in units of Ω and through Euler's equation is represented by a complex equation with real and imaginary parts. Graphically these parts can be represented by a Nyquist plot which has a real x-axis, an imaginary y-axis, and each plotted value going generally from left to right represents a decrease in the frequency of the voltage/current of the system (see **Figure 8** a) [46]. Alternatively, the information can also be represented by a Bode plot which explicitly represents the frequency on the x-axis with phase angle and impedance magnitude making up the y-axes (see **Figure 8** b). The shape of the Nyquist and Bode plots corresponds to specific electrochemical interface characteristics of the system.

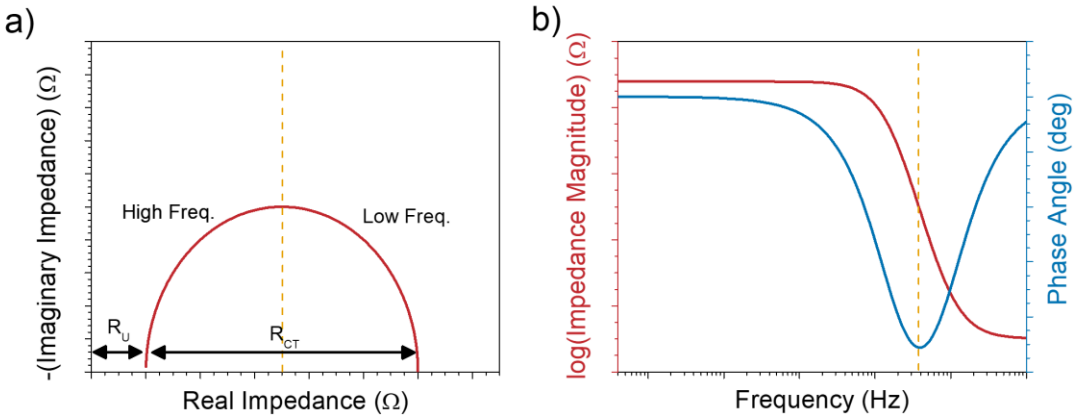

Figure 8. Examples of a simple a) Nyquist plot and b) Bode plot.

In this technique, certain trends pertain to a behaviour analogous to elements of an electric circuit. Thus, an equivalent model circuit is set up to represent the behaviour of the system based on the observed element. The models and their elements are based on real phenomena occurring in the cell and have trends that match certain system types (e.g. corrosion/coatings tests, battery tests, supercapacitor tests, etc.). The two major elements represent two general interface options for charge in an electrochemical system: resistance which represents charge movement across an interface, and capacitance which represents charge collection at an interface [46]. These are represented by the resistor (R) and capacitor (C) in the equivalent circuit model respectively. Additionally, inductance represented by an inductor (L), is also a common element to observe which represents the inductance of the instrument wires attached to the electrode at high frequencies and coupled electrochemical reactions by intermediates adsorbed on the electrode at low frequencies [46]. From these fundamental real analogous elements, more specific mathematically

derived elements can be used as tools to represent the complexity of the system. The Warburg element (W) is used to represent the mass transport of particles that participate in the electrochemical reactions to the electrode surface (e.g. ion diffusion). The constant phase element (Q) is used to represent the non-ideal capacitor whose behaviour can be adjusted to have resistor and Warburg characteristics [46].

The fundamental combination of elements in many electrochemical systems is the Randles circuit (see **Figure 9**). In it, the resistance of ions in the solution (and resistance in the instrument circuitry) are represented by the initial gap of resistance in the Nyquist plot. This resistance is called R_u for uncompensated resistance between the working and reference electrode in a three-electrode cell or R_s for solution resistance in a two-electrode cell. This is followed by a semicircle whose diameter represents the charge transfer resistance (R_{CT}) of the electrode. That is the resistance associated with the occurrence of electrochemical reactions. The imaginary contribution resulting in the height of the semicircle is due to the electric double-layer capacitance (C_{dl}) occurring on the electrode in parallel with R_{CT} in the equivalent circuit. Finally, in series with the R_{CT} is the Warburg impedance (Z_W) which defines the sloped line describing the ion diffusion in the cell [46]. Although ZIBs have equivalent circuits that deviate slightly from the fundamental Randles circuit, the elements describing the cell phenomena provide much insight into the inner workings of the cell. It is also important to note that an actual experimental cell undergoing EIS would be subjected to AC oscillating at a potential (such as OCP) with a particular voltage amplitude for a set range of frequencies. The recorded data from the experiment could be plotted on a Nyquist plot and fitted using an equivalent circuit.

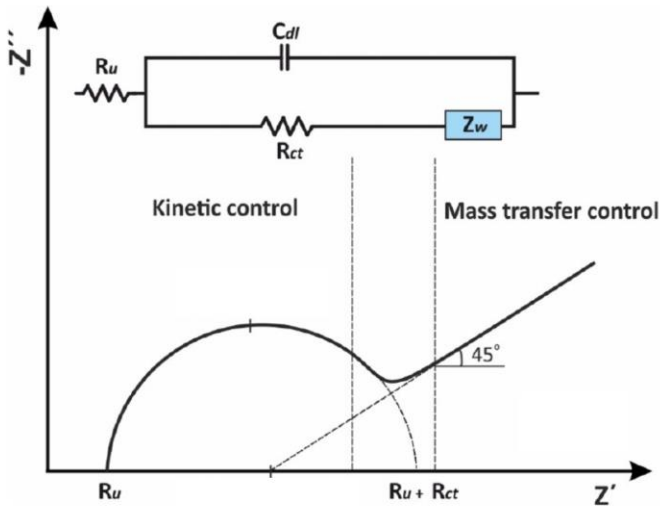

Figure 9. Equivalent circuit and Nyquist plot of a Randles circuit, adapted from [46].

2.6 Fourier Transform Infrared (FTIR) Spectroscopy

FTIR is a common infrared spectroscopy technique that detects functional groups in organic molecules. In general, it works by beaming infrared radiation at a sample which causes bond vibrations between atoms that reflect the chemical nature of the bond. This could be bond bending or stretching with two or more atoms. The specific bond vibration will occur at a precise wavenumber associated with the infrared signal which will be recorded as a peak in absorption of the signal or a dip in transmission at that wavenumber on the whole analysis spectrum (see **Figure 12**) [47]. The peak broadness can also reveal characteristics of the bond in question, as some peaks are expected to be broad while others are narrow. Peaks occurring in wave numbers in the fingerprint region (1500 cm^{-1} to 600 cm^{-1}) are more difficult to isolate so often peaks with larger wavenumbers are used to make initial general observations of the material [47]. The intensity of the peaks can qualitatively represent the amount of molecules with a functional group corresponding to that peak although further analysis would be needed to quantify the amount. FTIR in general is a qualitative technique to give quick insight into the possible chemical groups present. FTIR can be run using samples such as liquids or powders loaded on a stage with Attenuated Total Reflectance (ATR) subjected to a few scans of infrared radiation to quickly develop a spectrum of the material for analysis.

2.7 Thermogravimetric Analysis (TGA)

TGA is a material characterization technique that heats the material to a high temperature while recording the material's mass to highlight the loss of mass due to material decomposition at particular temperatures. Although there are a few configurations, TGA involves the placement of a heat-resistant pan containing the sample of interest on a sensitive microbalance, which is heated by a small furnace. The sample environment is subjected to a purge gas to carry away volatiles from decomposition. Commonly air (oxidizing) or an inert gas like argon is used during testing. Since the density of the purge gas will decrease as the temperature increases, the TGA system needs to compensate for the buoyancy change to eliminate a false mass gain that would be observed [48]. The results of TGA testing are often represented in a thermogram that demonstrates weight loss compared to the original weight on the y-axis and temperature on the x-axis (see **Figure 13**). In general below 150 °C weight loss is associated with the loss of small volatiles, trapped gases, and importantly water (through evaporation) [48]. Above that, mass loss due to evaporation and decomposition of less volatile materials starts to take place. The sharp decrease in weight during TGA at a particular temperature signals a physiochemical process associated with the loss of particular materials [48]. Thus, one can identify different chemical components of their material by correlating clear drops in weights with the predicted thermal stability of possible components knowing the chemistry of those components.

3. Project Investigation

The following is copy of the manuscript investigating the research project presented in this thesis. Herein the results from this investigation are presented and discussed. The appendix of this thesis document contains the supporting information for this manuscript. The manuscript has the same title as this thesis and is currently a private communication document, until a modified version of it has been submitted to a journal for future publication. Thus, it is referenced as *Private Communication from Thomas Baker: Dept. of Chemical Engineering, McMaster University, 2024*.

Development of Stabilized Organic Cathodes via Grafting Redox-active Molecules to Carbon in Aqueous Zinc-ion Batteries for Energy Storage Systems

Thomas J. Baker [a], Alejandra Ibarra Espinoza [a], Storm W Gourley [a], Brian D. Adams [a,b], Drew Higgins [a*]

[a] Department of Chemical Engineering, McMaster University, 1280 Main Street West, Hamilton, Ontario, L8S 4L7, Canada.

[b] Salient Energy Inc., 21 McCurdy Avenue, Dartmouth, Nova Scotia, B3B 1C4, Canada.

3.1. Abstract

Organic molecules such as 9,10-phenanthrenequinone (PQ) have shown much promise as active material for cathodes in aqueous zinc-ion batteries (ZIBs) due to their flexible and adaptable designs. However, they are prone to inactivation resulting in capacity fade throughout their operational lifespan. One technique used to stabilize quinone cathodes is to form a covalent bond between the organic molecule and conductive carbon substrates of the cathode by *in-situ* generated diazonium salt reactions. Fixing the molecule to the substrate inhibits its dislocation and electrochemical inactivation. Although explored for other battery chemistries (*e.g.,* Li-ion), this work probed the effectiveness of applying this chemical grafting technique to stabilize PQ on carbon black substrates in ZIB cathodes. PQ was simply grafted to Ketjenblack (KB) and Vulcan Black (VB) substrates and tested as a cathode material compared to PQ adsorbed on the substrates. It was found that grafted PQ-KB maintained a discharged capacity of 99 mAh g^{-1} after 1000 cycles of accelerated testing at charge/discharge rate of 200 mA g^{-1} and 10 mA g^{-1}. The PQ-KB cathode was stabilized by the grafting procedure retaining 67% of the discharged capacity compared to the 55% retained by cathodes with only adsorbed quinones. The PQ-VB cathode similarly maintained a 90 mAh g^{-1} discharge capacity which corresponded to 71% retention compared to 40% seen with adsorbed PQ on VB. This work not only emphasized the significance a carbon substrate can have on organic cathode behaviour, but also demonstrated how grafting organic materials to a carbon substrate is a simple modification that improves organic cathode performance in ZIBs.

3.2. Introduction

With the growing threat of climate change and continually rising greenhouse gas emissions from the global power sector, demand for green electricity generation has been greater than ever. As a result, the development and implementation of renewable power sources has been accelerated in many countries to decarbonize electricity production and meet carbon emission targets such as the Net Zero scenario[49]. However, the intermittency of these power sources necessitates the development of large-scale energy storage systems for electricity grids. Although currently accounting for only 2% of the global energy storage capacity, batteries are increasingly being sought after for grid-scale energy storage systems due to their flexible implementation and high energy density [4], [7]. Specifically lithium-ion batteries (LIBs) are being implemented for grid-scale energy storage as they have excellent energy density, relatively high cell voltage, and low self-discharge losses [8]. However, the production and use of LIBs comes with many challenges including high costs, material acquisition ethical concerns, and significant risk for thermal runaway [8]. Thus, new battery chemistries which can tackle these issues are being actively researched. Aqueous zinc-ion batteries (ZIBs) are one such chemistry, which operate through a similar reversible mechanism as LIBs. ZIBs can be made of much more abundant materials, have an increased level of safety owing to their air and water stable components, and have high theoretical anodic capacities of 820 mAh g^{-1} [6], [12].

The standard choice of cathode material for ZIBs has been mixed metal oxides (MMO) including layered inorganic compounds such as MnO_2 and V_2O_5. Owing to their

ability to reversibly intercalate Zn^{2+} within the voltage stability window for aqueous electrolytes ($\leq$ 2.0V vs Zn/Zn^{2+}), many MMOs have successfully demonstrated their practical utility for ZIB cathodes [13]. However, MMOs are susceptible to Jahn-Teller distortion and other phenomena during operation of the battery, which deteriorates the structure and reduces the charge storage capability of the material. Additionally, MMOs still rely on mineral extraction which is more vulnerable to supply-chain limitations and can reduce the sustainability of ZIBs [12]. Alternatively, organic-based cathodes have the potential for facile production and structure modification for optimized ZIB cell design.

Quinones are a class of redox-active organic molecules consisting of aromatic rings functionalized with at least two carbonyl groups that can be electrochemically reduced and protonated into alcohol groups [18]. When incorporated as an organic-based cathode the molecule can be stabilized via adsorption to carbon substrates using π-π intermolecular interactions between the aromatic rings of the quinone and the carbon [18]. This allows for quick charge transfer which makes quinones an ideal material for supercapacitor and battery electrode applications. For example, Anjos *et al.*, designed supercapacitor electrodes from carbon onion substrates and a variety of quinones such as 1,4-naphthoquinone, 9,10-phenanthrenequinone (PQ), and 4,5-pyrenedione [19]. This small molecule adsorption technique has similarly been employed for a variety of quinones and carbon substrates in supercapacitor development including 9,10-anthraquinone (AQ) on Ketjenblack (KB), hierarchical porous carbon nanotubes, and highly porous graphitic carbon fibres [20]–[22]. This work was also inspired by previous supercapacitor success in utilizing PQ adsorbed to porous nitrogen-doped reduced graphene oxide [50]. This

translates well to battery electrode development, specifically ZIB cathode design. Due to the flexible organic structure and ≥2 electronegative groups found in most quinones, they can coordinate well with divalent ions like Zn^{2+} enabling this charge storage mechanism in addition to protonation [5]. As a result, quinones have become a material of interest for ZIBs with molecules such as calix[4]quinone and tetrachloro-1,4-benzoquinone having been demonstrated to work effectively as ZIB cathodes [51], [52].

However, despite these advances quinone-adsorbed electrodes suffer greatly from capacity fade during charge and discharge operation. Capacity fading has been seen in ZIBs, LIBs, and supercapacitor electrodes [5], [38], [53]. Traditionally, this fade was attributed to molecule dissolution during cycling, but recent work suggest that the capacity loss may be caused by uncontrolled phase changes in the organic layer of the cathode [5], [26]. For example, it has been proposed that Oswald ripening causes the protonated quinones to grow electrochemically inactive crystals, that do not participate in future charge storage [28]. There have been many different approaches to stabilizing redox active organics in electrodes. Gao *et al.*, synthesized covalent organic frameworks out of 2,7-diamino-PQ and pyrene-4,5,9,10-tetrone (PYT) that maintained a higher-level structure resilient to degradation during cycling when tested on carbon nanotube substrate for LIB cathodes [53], [54]. Other studies have stabilized quinones by polymerizing them into redox active chains. For example, the work done by Nokami *et al.*, was able to polymerize PYT for LIB cathodes while Guo et al. made Poly(quinone-1,4-diamino-AQ) for ZIB cathodes [25], [55]. The results from these studies are promising but often employ synthesis pathways that can quickly become complicated or intensive. As such, another approach to

stabilizing redox-active organics has been directly grafting the organic molecule to the carbon substrate.

There are a variety of reactions that can be used to anchor organic molecules on carbon substrates like graphene, and carbon blacks, including amidation, esterification, and diazonium modification. Diazonium salt grafting is particularly interesting as it allow the addition of molecules perpendicular to the carbon surface [29]. Since carbon black is inexpensive and relatively simple to manufacture, using it as a carbon substate in ZIB cathodes sustains the inexpensive nature of ZIB design. As such, there has been extensive history employing diazonium chemistry to undertake this grafting process with carbon black [29]. For example, Jaffe *et al.*, were able to graft and stabilize small quinones (PQ, AQ, and PYT) on the surface of KB and increased capacity retention after 500 cycles of the PQ and KB cell from ~34% to 71% in LIBs [38]. A major inspiration for this work come from the chemical and electrochemical grafting of quinone molecules to carbon substrates via *in-situ* generated diazonium salts for supercapacitor electrodes done by Le Comte *et al.*, [35], [36]. The work presented tunable electrochemical grafting and non-chemically intensive spontaneous chemical grafting techniques that increased electrode stability which fulfills many of the manufacturing desires of sustainable ZIBs [35]. However, to the best of the authors' knowledge grafting quinones to a carbon substrate has not been reported for ZIB cathodes.

In this work, PQ was chemically grafted to two types of carbon black: KB and Vulcan Black (VB) via a facile diazonium modification procedure and tested as cathode materials for aqueous ZIBs to study their performance for grid-scale storage orientated

design (**Figure 10**). The material changes induced by the grafting were observed via Fourier Transform Infrared (FTIR) spectroscopy and Thermogravimetric Analysis (TGA). The material was prepared into a ZIB cathode and subjected to electrochemical testing including battery charge-discharge testing. The grafted PQ cathode was compared to traditional non-grafted (adsorbed) PQ, and it was found that the grafted PQ-KB ZIB cells achieved a capacity of 99 mAh g^{-1} and a capacity retention of 67 % over 1000 cycles of accelerated testing at a charge/discharge rate of 200 mA g^{-1} and 10 mA g^{-1}. Under the same testing conditions, the grafted PQ-VB cathode was also able to achieve a 90 mAh g^{-1} discharge capacity which corresponded to 71% retention. The practical improvement to cell stability highlights how better organic cathode performance can be achieved in ZIBs through this facile modification.

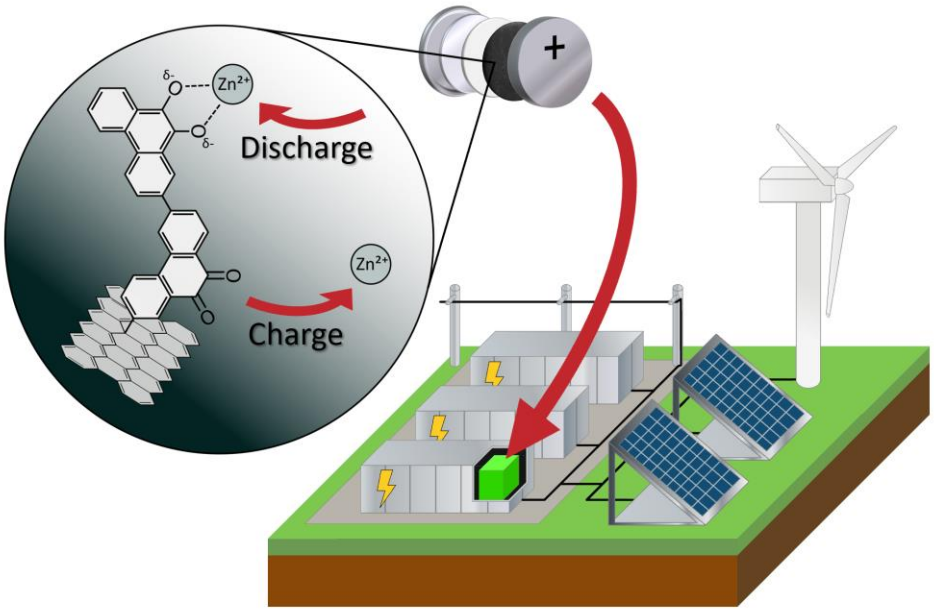

Figure 10. Schematic of grafted organic cathode ZIB battery operating in grid scale energy storage with inset showing zinc coordination with quinone molecules covalently grafted to a carbon support.

3.3. Experimental Methods

3.3.1. Materials

Ketjenblack EC-300J in agglomerates of 100 μm and with surface area of 800 m^2 g^{-1} (KB) was obtained from the Fuel Cell Store. Vulcan Black XC 72R with surface area of 240 m^2 g^{-1} (VB) was obtained from Cabot Corporation. 9,10-phenanthrenequinone (≥99.0%) was obtained from TCI America. Polytetrafluoroethylene (PTFE) was purchased from Sigma-Aldrich.

3.3.2. Cathode Synthesis Procedure

The synthesis procedure of the grafted quinone precursors (Steps 1 and 2, see **Figure 11**) was adapted from [36], [38].

Step 1) Formation of nitro-9,10-phenanthrenquinone (PQ-NO_2)

To functionalize PQ with a nitro group, 4.0 g of PQ was combined with 110 mL 70% HNO_3. The mixture was heated to 130 °C in an oil bath and stirred for 50 minutes. The red mixture was then poured into 250 – 500 mL of ice which induced the precipitation of a bright orange solid. The mixture stood in rest for 45 minutes, the solids were separated via vacuum filtration, and they were dissolved in 250 mL of refluxing glacial acetic acid (stirred at 300 RPM) to form a solution that was just saturated. It was cooled to room

temperature for the recrystallization of nitro-9,10-phenanthrenquinone molecules which came out of solution. The mixture was then vacuum filtered obtaining 1792 mg of solid nitro-9,10-phenanthrenquinone.

Step 2) Formation of amino-9,10-phenanthrenquinone (PQ-NH_2)

500 mg of nitro-9,10-phenanthrenquinone and 2.1 g of sodium hydrosulfite were mixed together in a 500 mL round bottom flask. 170 mL of 1.5 M sodium hydroxide was then added, and the solution was stirred at 300 RPM, and purged with nitrogen gas. The flask was then submerged in a water bath, heated to 65 °C, and stirred for 15 minutes. During that time the solution went from turning initially green to brown in a few minutes with no solids visible by the end of the 15 minutes. The solution was removed from the bath/heat, diluted 2.6 times with room temperature DI water (270 mL), and bubbled with air for 15 minutes. A black precipitate formed during air bubbling which was recovered through vacuum filtration. The solid was dissolved in 60 mL of refluxing ethanol, to get a just saturated solution. Finally, the mixture was cooled to room temperature allowing for amino-9,10-phenanthrenquinone to recrystalize. The solids were then extracted via vacuum filtration.

Step 3) Chemical Grafting

This procedure follows what was described as an optimum chemical grafting procedure for 2-aminoanthrenquinone done by Le Comte *et al*. [35]. KB and VB were used for grafting, generalized here as carbon black (CB). The grafting was performed with 60 mg of PQ-NH_2 mixed with 30 mg of CB (2:1 ratio). The PQ and CB were mixed with 10 mL of ethanol and sonicated for 1 hour to adsorb the quinone to the carbon. The suspension was then poured into a beaker of 200 mL of a 0.1 M H_2SO_4 solution. Then 1380 mg of $NaNO_2$ was added to make a 0.1 M $NaNO_2$ solution in the beaker. The spontaneous grafting reaction occurred as the materials were mixed at 400 RPM for 24 hours at room temperature[35]. The grafted material was then extracted with vacuum filtration and washed with several aliquots of ethanol.

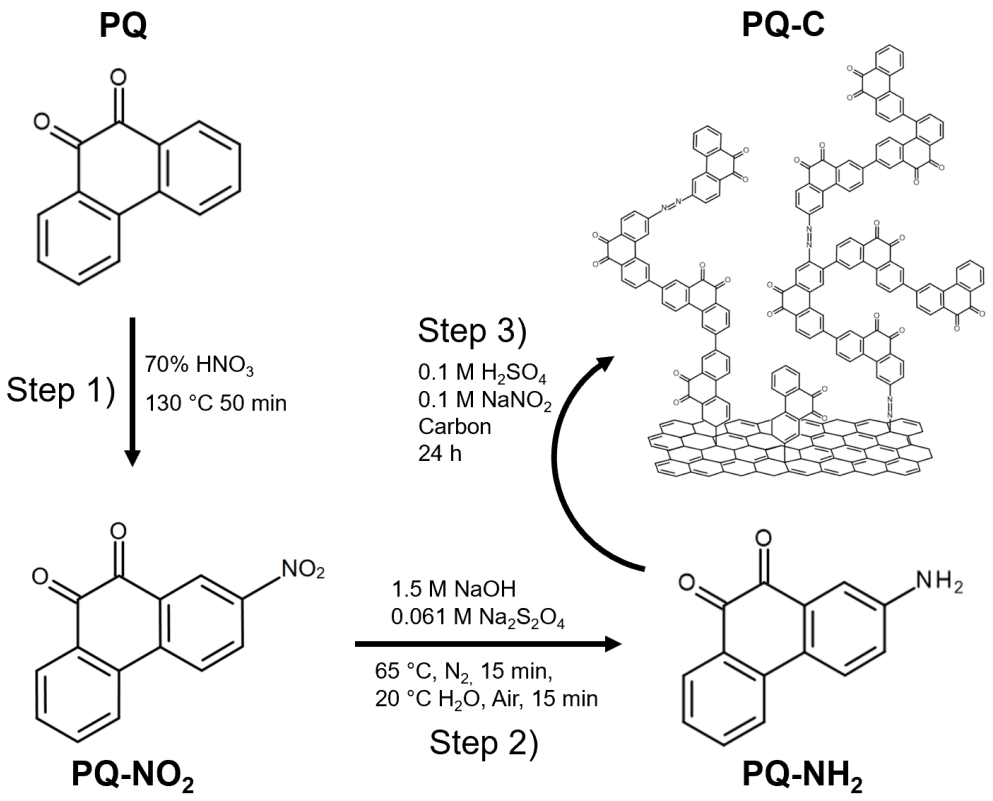

Figure 11. Synthesis procedure for forming 9,10-phenanthrenequinone precursors and grafting them to carbon substrate.

3.3.3. Cathode Synthesis and ZIB Assembly

All cathode materials (grafted or absorbed) started with an initial mass ratio of 6:3:1 (PQ: CB: PTFE), however, the grafted material was washed with ethanol which removed some PQ and caused the ratio to change to 4:5:1. The cathodes with PQ absorbed on CB were formed by sonicating PQ and CB in ethanol for one hour before mixing in PTFE (6:3:1 mass ratio). Ethanol was added as needed to disperse the cathode materials. The slurries were mixed for 6 minutes at maximum rotation and revolution speed in a Mazerustar KK-250S mixer until smooth and flowable. The slurries were then poured onto 15 cm × 10 cm sheets of carbon paper and coated to a thickness of 150 μm via doctor blade. The electrode was allowed to dry at room temperature for 30 min.

Individual cathode disks of ½″ diameter were punched out of the loaded carbon paper. The mass difference between the carbon paper and loaded carbon paper determined the per cathode material loading. The cathodes had approximate loadings of 0.4 mg cm^{-2} – 1.0 mg cm^{-2}. The electrodes were then assembled into coin-cell type batteries. CR2032 coin cells were assembled using the cathode, a $^{9}/_{16}$″ diameter zinc metal (0.2032 mm thick, McMaster-Carr) anode, and a ⅝″ diameter glass fibre separator (grade GF/D, Whatman). 150 μL of 1 M $ZnSO_4$ electrolyte was added to the cell.

3.3.4. Electrochemical testing

The coin cells were tested using a BTS-4000-5V100mA battery cycler from NEWARE Technology LTD in at least duplicates. The cells were cycled between 0.5 V and 1.3 V vs Zn/Zn^{2+} via accelerated testing. That is, the cells were cycled at a slow rate of 10 mA g^{-1} for the first, second, and every twentieth cycle. This is known as a reference performance test (RPT). The rest of the cycles were performed at a high current density of 200 mA g^{-1}. In another cycling test, the cells were also cycled between 0.5 V and 1.3 V vs Zn/Zn^{2+} at a consistent slow rate of 10 mA g^{-1} for 100 cycles. All the cells rested for 3 hours at open circuit voltage (OCV), were fully discharged, and then cycled. So, the second discharge to occur was considered the initial discharge for performance analysis.

Rate Capability Testing (RCT) was performed on cells utilizing the same battery tester. The cells were conditioned for 10 cycles at a slow current density of 10 mA g^{-1} and then tested under 10, 30, 50, 100, 200, 1000, and back to 10 mA g^{-1} for 5 cycles each. Additionally, Galvanostatic Intermittent Titration Technique (GITT) testing also utilized the same battery tester. After one charge/discharge cycle, the cells were pulsed with a 100 mA g^{-1} current density for 2 minutes followed by a rest period at OCV for 30 minutes. This process was repeated until the cells stabilized at their discharge voltage of 0.5 V. The coefficient for Zn^{2+} in the ZIB cells was calculated using the collected electrochemical data, and the tap density of the adsorbed samples at the 6:3:1 and 4:5:1 ratios (assumed to be applicable for all samples).

Cyclic Voltammetry (CV) testing was performed on the coin cells via a BioLogic VSP-300 Multipotentiostat. For CV testing the cells were cycled between 0.5 V and 1.3 V vs Zn/Zn^{2+} at 0.1 – 10.0 mV s^{-1} for 2 – 20 cycles. Electrochemical Impedance Spectroscopy (EIS) testing was carried out on the coin cells using the same potentiostat. After letting the cells soak for 3 days, the testing was performed from a frequency of 1 MHz to 4 mHz at the cells' OCV with a 10 mV amplitude, recording 6 points per decade.

3.3.5. Material Characterization

Fourier Transform Infrared (FTIR) spectroscopy was performed via a Nicolet 6700 FTIR Spectrometer with an Attenuated Total Reflectance (ATR) attachment in a spectrum range of 4000-500 cm^{-1}. Thermogravimetric Analysis (TGA) was performed on the cathode materials and precursors via a Mettler Toledo TGA/DCS 3+ instrument. The powder samples were heated to 1000 °C at a rate of 10 °C min^{-1} under an air flow rate of 30 mL min^{-1}. Scanning Electron Microscopy (SEM) was performed via a Thermo Scientific Quattro ESEM courtesy of the Canadian Centre for Electron Spectroscopy (CCEM). Mass Spectroscopy (MS) tests were performed with a Micromass/Waters Quattro Ultima Triple Quadrupole Mass Spectrometer using APCI (Atmospheric Pressure Chemical Ionization).

3.4. Results and Discussion

In the spontaneous grafting process nitrite ions were reduced in the acidic media leading to the formation of diazonium groups on the quinones replacing the amine groups [35]. The diazonium groups were unstable and spontaneously reacted to create a radical on the quinone, while the diazonium salt was reduced to nitrogen gas and bubbled off [30], [33]. This radical then formed a covalent bond with the adjacent sp^2 hybridized carbon (KB or VB) completing the grafting process. The diazonium group may also bare the radical instead of leaving leading to grafting through azo linkages. Overall, these processes can lead to the grafting of individual quinones to the carbon [33].

However, oligomer chains of the quinone formed by azo linkages and diazonium induced bonding to adjacent quinone's aromatic groups are also expected to form, see **Figure 11** [33], [38]. It was hypothesized that in the grafting process performed in this work some oligomer chains of PQ did not bond to carbon black. This necessitates the washing step of the post grafted material to remove most of the unbonded quinone (residue) which may have been absorbed on the carbon black. Although it could be hypothesised that the residue washed away from the grafted material was unreacted PQ-NH_2, there is evidence to suggest otherwise. For example, the colour of the residue (yellow-orange) was different from the immediate precursor PQ-NH_2 colour (violet), suggesting a chemical reaction occurred even on the quinones that failed to graft. This is further backed up by FTIR analysis (**Figure S1 a**) which shows a lack of amino group peaks found in PQ-NH_2.

As seen in **Figure S1 b**, the mass spectrometry analysis suggests that majority of material that failed to graft reverted back to monomeric PQ with a small presence of PQ dimers.

FTIR was used to further confirm the precursor material was synthesized and to give insight into the success of the grafting reaction. PQ has characteristic peaks at 1670 cm^{-1} and 1590 cm^{-1} corresponding to C=O bonds stretching which is highlighted in **Figure 12 a**, but can be seen in all quinone derivatives in **Figure 12**, including on the final grafted product (**Figure 12 d**) suggesting the presence of grafted quinone attached to the carbon surface [27]. In **Figure 12 c** the peak at 1520 cm^{-1} is associated with nitro stretching. In **Figure 12 b**, the two peaks below 3500 cm^{-1} and the peak at 1650 cm^{-1} is associated with primary amine stretching and bending respectively [36], [47]. **Figure 12 b, c** confirms the correct functionalization according to the synthesis step 1 and 2. **Figure 12 d** lacks the distinct amino peaks which could suggest the lack of amino-quinone on the grafted cathode material. Finally, the small size of many of the peaks can be explained by the interference of signal due to the large amount of carbon in the measured cathodic material (**Figure 12 b-d**).

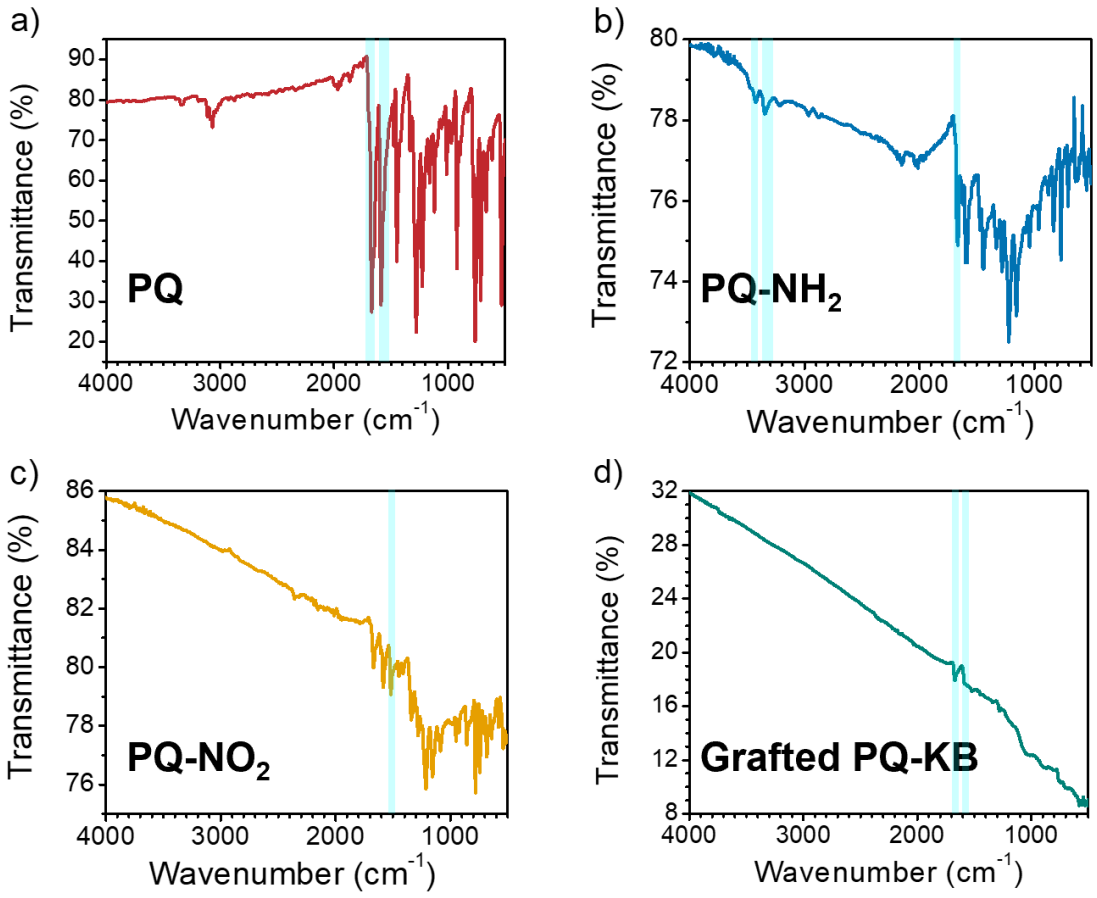

Figure 12. FTIR spectra of pristine PQ and cathode materials (quinone, KB, PTFE) with characteristic peaks highlighted in blue for a) Pristine PQ (C=O stretch), b) PQ-NH_2 (primary NH_2 stretching and bending), c) PQ-NO_2 (NO_2 stretching), d) chemically grafted PQ-KB (C=O stretch).

TGA was performed to understand how the cathode synthesis method affected thermal stability, highlighting the difference between adsorbed and grafted cathodes. **Figure 13** describes the weight loss for pure KB, pure PQ, absorbed PQ, and grafted PQ as temperatures were increased up to 1000 °C. The decomposition of KB started around 575 °C which was consistent with literature [56], [57]. Sublimation of PQ was reported at 200 °C which is in line with the observed data for pure PQ highlighted in **Figure 13** [58].

Logically, both adsorbed quinone on carbon and grafted quinone-carbon materials should have TGA plots between these extremes as a mixture of the materials. The >95% weight loss of the absorbed quinone past 200 °C is attributed to the destruction of stabilizing π-π interactions and the subsequent sublimation of PQ away from the carbon support. The remaining carbon followed a similar decomposition as the pure KB at higher temperatures. With the majority of the residual adsorbed PQ removed during the ethanol wash, the grafted sample only has a small decrease at 250 °C and instead has a notable weight drop at 500 °C and a final decrease at 600 °C due to the decomposition of the KB support. The notable weight drop at 500 °C is believed to be caused by the degradation of the grafted quinone chains which required more energy and thus a higher temperature to decompose due to the covalent bonding unlike the adsorbed PQ [36], [58]. This grafted decomposition temperature matches the decomposition temperature of previous grafted aromatics on carbon black [59]. The small drop at 250 °C on the grafted sample is associated with a small amount of remaining residual quinone adsorbed and stabilized in the nanopores of carbon, hence a slight increase in energy was required to remove these quinones compared to the pristine bulk and surface adsorbed quinone samples [28]. The thermal properties of VB are similar to KB and the TGA decomposition of KB lines up with previous VB decomposition results [59].

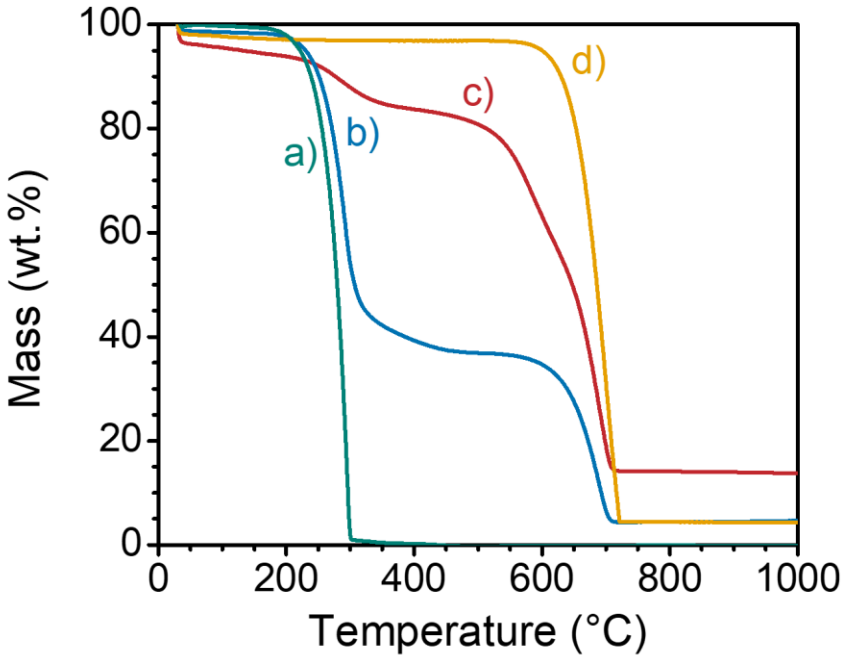

Figure 13. TGA curve of a) PQ, cathode materials b) adsorbed PQ to KB and c) chemically grafted PQ-KB, along with d) KB, ramped to 1000 °C at a rate of 10 °C min^{-1}.

SEM was used to analyze the microstructure and morphology of the prepared materials. It is clear from **Figure 14 a,b** that the slurry of cathode material layered the surface of the carbon paper current collector. However, in this granular coating before cycling, at this scale there seems to be no discernable difference between the grafted and adsorbed samples. This makes sense as homogenously spread quinone molecules grafted or absorbed in the porous carbon structures would be interacting on a much smaller scale. However, as seen in **Figure 14 c,d**, the charge and discharge state cathodes contained the presence of large flakey structures. These structures were believed to be Zinc Hydroxy Sulfate (ZHS) which was expected to form on the cathode in the discharge state of ZIBs, and some also remained in the charged state of these cathodes [60].

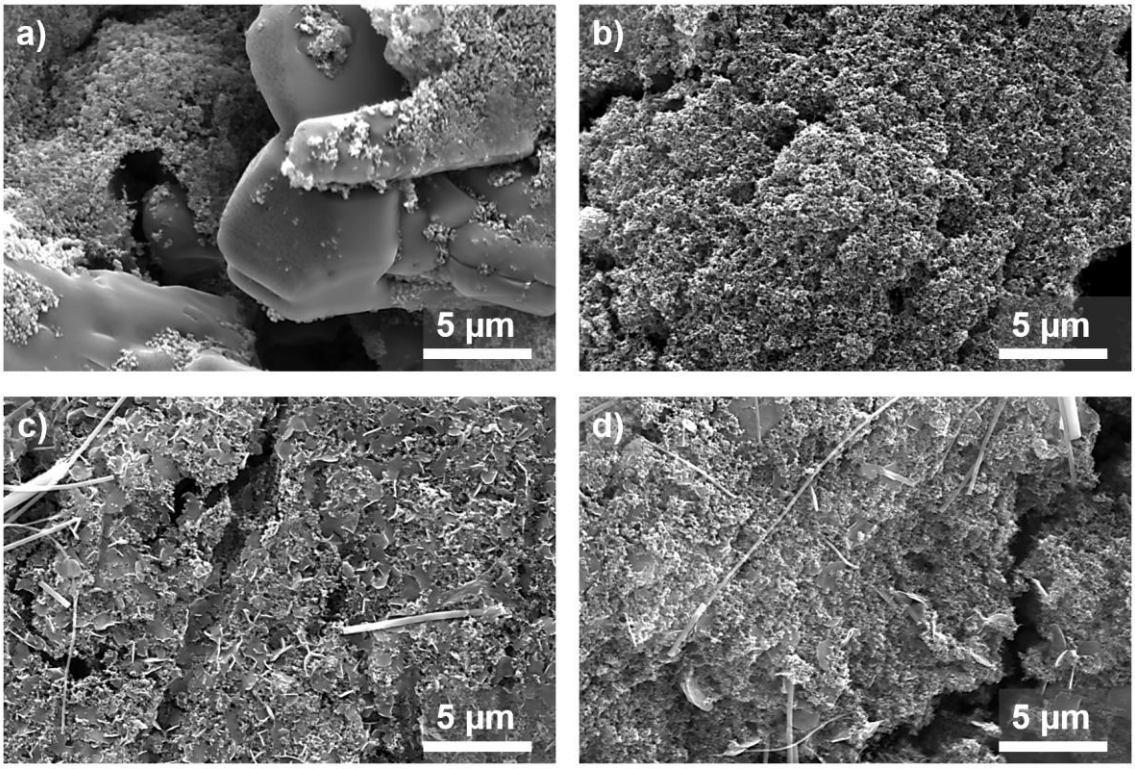

Figure 14. SEM images of a) pristine adsorbed PQ on KB cathode, b) pristine chemically grafted PQ-KB cathode, c) chemically grafted PQ-KB cathode after the first charge d) chemically grafted PQ-KB cathode after the second discharge.

As seen in **Figure 15** grafted quinones demonstrated mainly one broad redox peak in CV, amalgamating the smaller peaks that are highlighted on the adsorbed samples. The presence of the smaller peaks for the adsorbed PQ on carbon is consistent with what is seen in literature for similar material ratios [52]. The broadening of the peak can be explained by the formation of a grafted interface layer of exposed quinone groups with electrolyte interaction that dominates electrochemical signal. As seen with the higher charge transfer resistance (R_{CT}) in the EIS data (**Figure 17**), below this layer it would be expected to have

slower charge transfer interactions that could broaden this peak. This is consistent with the formation of a grafted layer on a conductive support previously seen with PQ [38], [61].

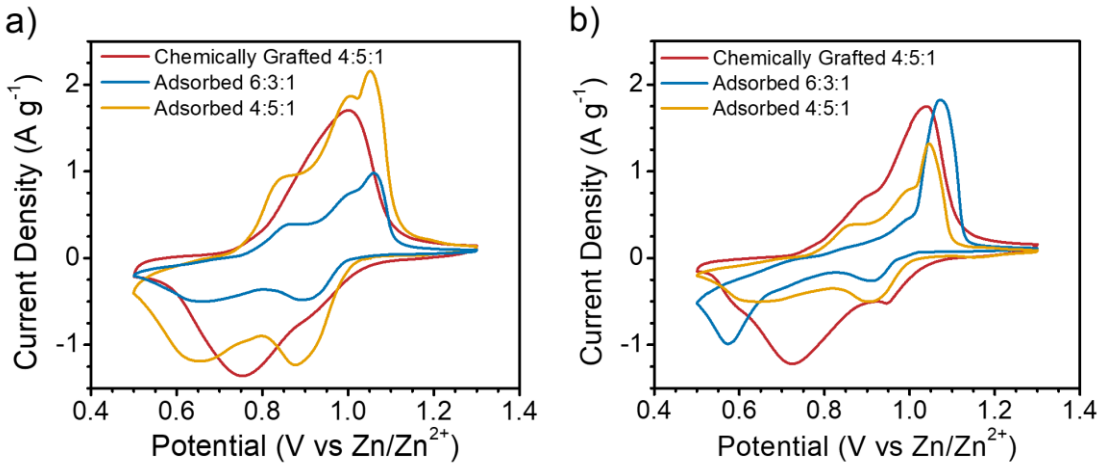

Figure 15. CV curves of cathode materials (PQ:CB:PTFE) at 1 mV s^{-1} for chemically grafted PQ 4:5:1, and adsorbed PQ on the carbon black substrate with 6:3:1 and 4:5:1 material ratios for a) KB and b) VB.

Literature has shown that PQ in ZIB can be controlled by a diffusion process [52]. This can be determined by *b*-value analysis which relates maximum peak height to scan rate by the following equation:

$$I_P = a\nu^b \qquad \text{(Eqn. 1)}$$

Where I_P here is taken as the oxidation peak (mA), ν is the scan rate (mV s^{-1}) and *a*, *b* are coefficients. When $b = 1$ the process is surface controlled by either capacitance or surface redox processes and when $b = 0.5$ the process is diffusion controlled [40]. If *b* falls is between 0.5 and 1, then the process could be a combination of the two controls [40]. This analysis was done using the oxidation peak (1.0 – 1.2 V vs Zn/Zn^{2+}) which has consistent

and clear representation in all samples (See **Figure 15**). Since the calculated *b*-value for all samples falls between 0.5 and 1, both diffusion and surface redox/capacitance mechanisms are occurring (**Figure 16**) [40], [44]. The obtained *b*-values were near to those reported previously for similar battery chemistries [55], [62]. Additionally, the surface-exposed grafted chains tend to consistently have larger *b*-values which understandably mean those quinones react more in a surface process.

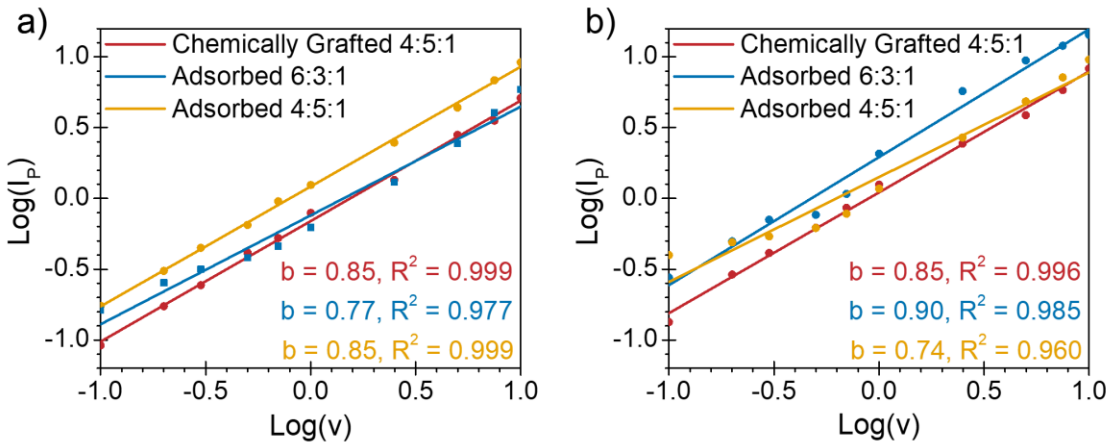

Figure 16. Linear fit of relations derived from CV between scan rate (ν) and peak oxidation current (I_P) for b-value analysis for chemically grafted PQ 4:5:1 (PQ:CB:PTFE), and adsorbed PQ on the carbon black substrate with 6:3:1 and 4:5:1 material ratios for a) KB and b) VB.

In **Figure 17**, the Nyquist plots of the cathode samples are displayed. The shape of the EIS Nyquist plots is consistent with literature for PQ in ZIBs [27], [63]. The formation of a grafted, less conductive layer on the surface of the carbon has been shown to yield a higher charge transfer resistance as seen by the semicircle width in the Nyquist plot (**Figure 17**) [37]. An equivalent model circuit (**Figure S3**) was created following similar literature

testing procedures [46], [52]. The R_{CT} values were calculated to be 1200 Ω, 300 Ω, and 1275 Ω for the KB grafted, adsorbed 4:5:1, and adsorbed 6:3:1 samples respectively. On the other hand, the VB samples had R_{CT} values of 1150 Ω, 1100 Ω, and 1020 Ω for the grafted, adsorbed 4:5:1, and adsorbed 6:3:1 samples, respectively. The charge transfer resistances of the grafted PQ were consistently larger than the adsorbed PQ for the same 4:5:1 material ratio on both KB and VB (see **Figure 17**). The adsorbed PQ on KB sample of 6:3:1 had a larger charge transfer resistance compared to other KB samples which could be attributed to the high quantity of quinone molecules that cover most of the surface of the carbon, increasing resistance. For VB the lower R_{CT} of the adsorbed PQ 6:3:1 sample may have to do with the lower carbon surface area, meaning that most of the quinones are aggregated rather than covering the entire surface of the carbon like they are with the higher surface area KB. The remaining active quinones in the adsorbed PQ on VB 6:3:1 sample also had a larger b-value which suggests that surface redox reactions play a more significant role for electrochemical performance than diffusion processes which were slowed by quinone aggregate formations on this less porous carbon substrate [20].

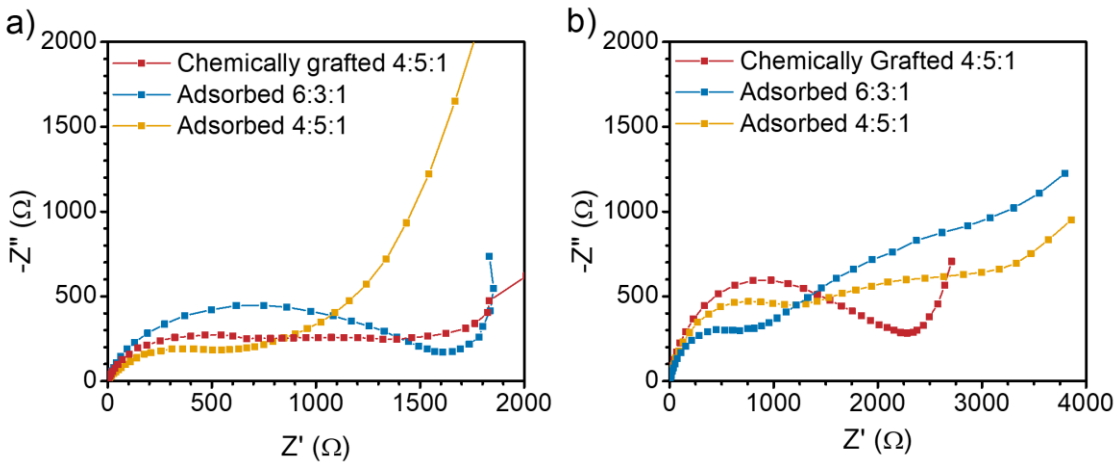

Figure 17. EIS Nyquist plots of chemically grafted PQ 4:5:1 (PQ:CB:PTFE), and adsorbed PQ on the carbon black substrate with 6:3:1 and 4:5:1 material ratios for a) KB and b) VB at OCP.

RCT was performed on all materials to highlight capacity changes as the current density increased. Previous work that investigated grafting quinones to carbon for other energy storage chemistries had similar RCT profiles to this work. Generally as an active material quinones have shown capacity decrease as charge/discharge rate increased [38], [58]. However, in previous literature, adsorbed PQ on carbon showed quick redox reactions when used in supercapacitor devices, demonstrating small capacity decreases at high current densities [19]. As seen in **Figure 18**, for both the KB and VB samples, the grafted and adsorbed cells showed capacity decrease as the current density was increased. However, the grafted quinones consistently maintained a higher capacity for each rate. From 10 mA g^{-1} to 1000 mA g^{-1} both grafted samples had a capacity drop of less than 30%. The grafted samples also had larger capacities at each rate than the adsorbed samples except for adsorbed PQ on KB 4:5:1 at low rates. This could be due to the fact that the grafted

quinones are in a more exposed position, so they have a better chance to react at higher rates than quinones adsorbed in the carbon pores.

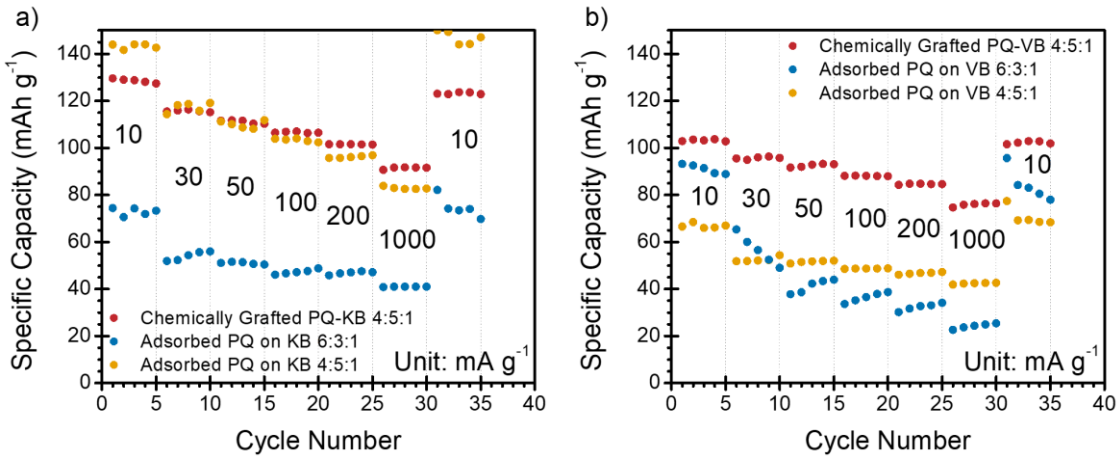

Figure 18. Rate capability testing with discharge capacities of a) KB supported cathodes and b) VB supported cathodes.

Grafted and absorbed PQ cells were cycled for 1000 cycles at an accelerated rate with a RPT every 20th cycle to validate operation. The use of accelerated testing allowed the evaluation of cells at realistic charge/discharge rates and allowed the cells to reach 1000 cycles in a reasonable timeframe. The discharge capacity and discharge capacity retention plots are shown in **Figure 19** and the performance metrics of the cells after accelerated cycling can be seen in **Table 1**.

Table 1. Accelerated cycling performance metrics for adsorbed and grafted cathodes (PQ:CB:PTFE). Error represents standard deviation of duplicate tests.

	Initial Discharge Capacity (mAh g^{-1})	Final Discharge Capacity (mAh g^{-1})	Capacity Retention (1000 cycles)	Columbic Efficiency	Round Trip Efficiency
PQ-KB (4:5:1)	148.3 ± 0.4	99.4 ± 0.1	67.0% ± 0.1%	100% ± 7%	82% ± 8%
PQ Adsorb KB (6:3:1)	161 ± 3	89 ± 2	55.4% ± 0.3%	99% ± 5%	81% ± 4%
PQ-VB (4:5:1)	120 ± 20	90 ± 10	71% ± 1%	100% ± 10%	80% ± 10%
PQ Adsorb VB (6:3:1)	120 ± 10	46 ± 8	30% ± 10%	100% ± 10%	80% ± 10%
PQ Adsorb VB (4:5:1)	210 ± 80	78 ± 5	40% ± 20%	100% ± 7%	84% ± 6%

As seen in **Figure 19 a, b** for the KB samples, the adsorbed PQ cells had a higher initial capacity but were less stable in the long run and faded to a residual capacity that was lower than for that of the grafted quinone (~99 mAh g^{-1} vs 89 mAh g^{-1}). This capacity fade is highlighted by the loss of total capacity in the charge and discharge curves seen in **Figure 20** with the adsorbed PQ curves matching those in literature [52]. The grafted sample has a gently sloped plateau rather than a flat one that is very consistent throughout all the cycles. This sloped plateau has been seen in previous work involving the grafting of PQ to KB for LIBs [38]. **Figure 19 c,d** highlights the accelerated cycling results of the PQ adsorbed and grafted on VB. As seen by this and the metrics in **Table 1**, the grafted PQ-VB cells had similar performance to the grafted PQ-KB cells. However, capacity retention was

significantly improved by grafting PQ to VB, with a >30% increase compared to the adsorbed PQ on VB cells.

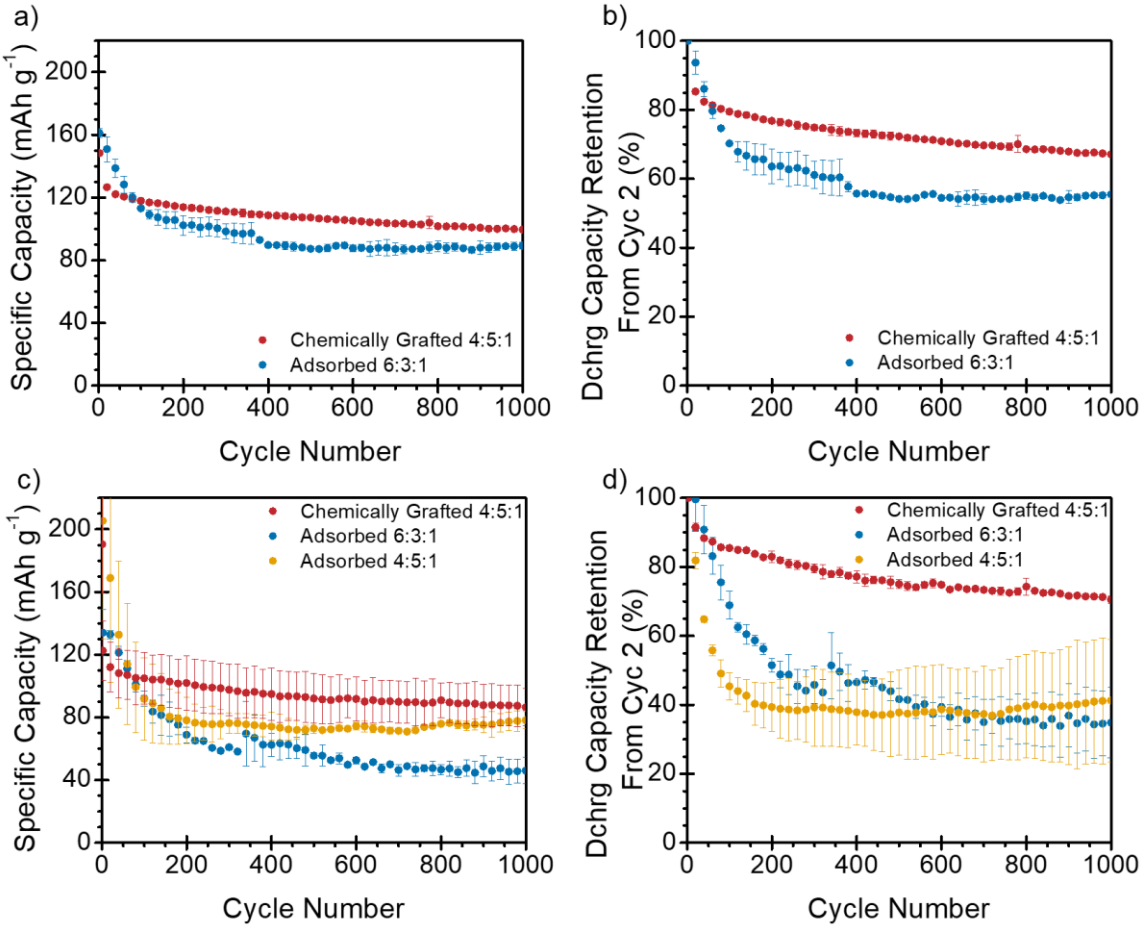

Figure 19. Accelerated cycling testing of cells with a RPT current density of 10 mA g^{-1} performed on KB supported cells (top) and VB supported cells (bottom) with a) & c) showing discharge capacity, b) & d) showing discharge capacity retention. Error represents standard deviation of duplicate tests.

Chemical grafting provided a >10% boost to capacity retention for the cells cycled in an accelerated test. Carbon type and pore availability also seem to play a role in stabilizing the adsorbed quinones. Tomai *et al.*, found that this could be explained by

nanopores (<100 nm diameter) in the carbon stabilizing quinones to allow the capacity to plateau at a residual value [28]. That is that adsorption in the pores seem to improve capacity retention possibly by limiting quinone inactivation through Ostwald ripening. Carbon that lacks this porosity, such as Vulcan Black, have greater stability issues when cycling (see **Figure 20** d). Zn^{2+} is a large sluggish ion that inherently has an increased electrostatic interaction volume due to its solvation shell in an aqueous electrolyte [64]. So, it requires good accessibility for an effective charge/ discharge process in the cathode. Grafted quinones on the other hand, do not need to be buried in nanopores to be stabilized allowing them to remain in exposed positions where they are openly accessible to interact with Zn^{2+}. Also, unlike non-grafted analogues, grafted quinones are not expected to desorb and reabsorb via Ostwald ripening during discharging and charging which has been previously reported [28]. These phenomena explain why the capacity quickly faded by >25% in the first 100 cycles for adsorbed quinones, as seen in **Figure 20**. The movement of quinones not stabilized by nanopores prevents consistent stable redox interactions, causing capacity to quickly fade to that residual capacity only provided by the groups buried within the nanopores. Cycling at slower, more practical rates is good practice to determine realistic stability, as fast cycling (>2C) does not provide long term stability performance that is relevant for targeted applications. As such, another cycling test was performed to see if the grafted quinones remained stable if subjected to many slow charge and discharge cycles.

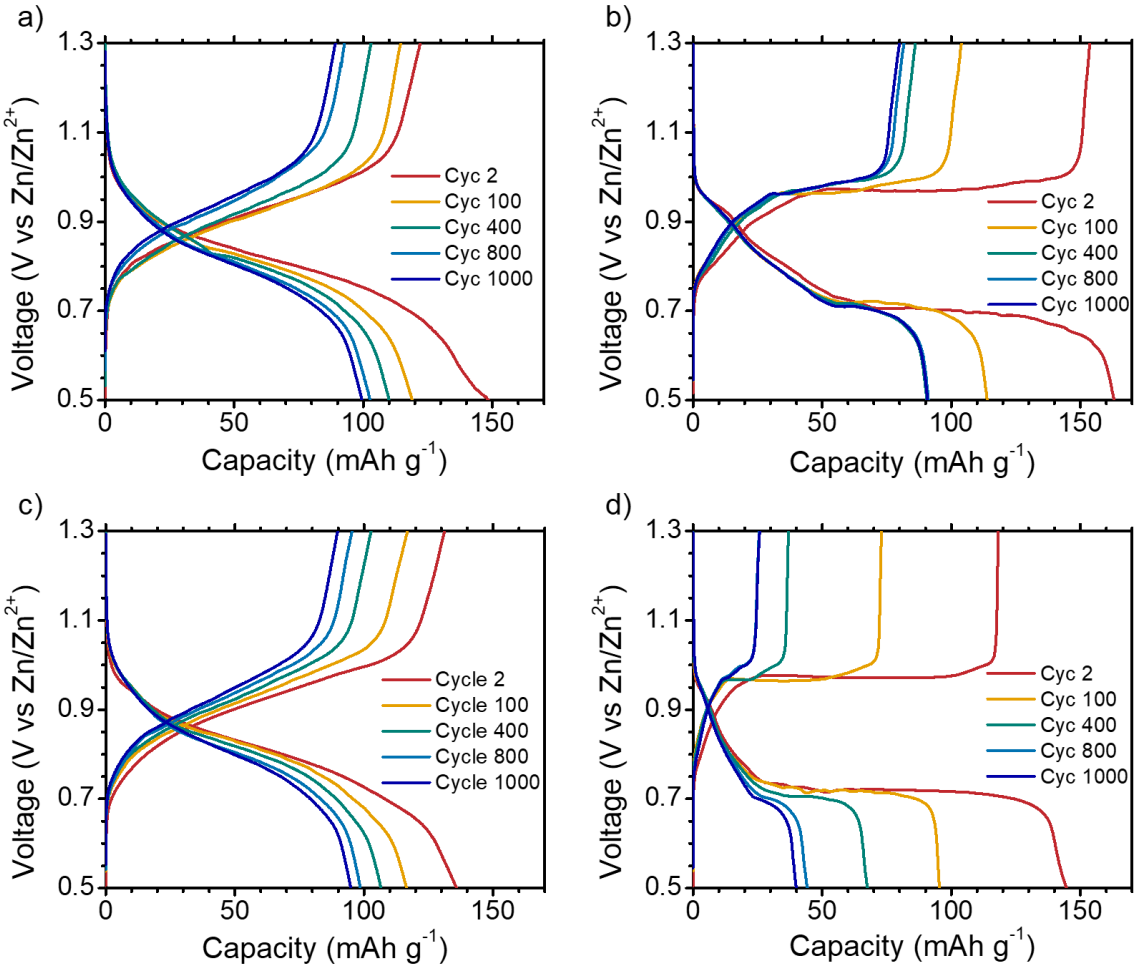

Figure 20. Charge and discharge curves for ZIBs with a) chemically grafted PQ-KB cathode, b) adsorbed PQ on KB cathode, c) chemically grafted PQ-VB cathode, and d) adsorbed PQ on VB cathode 6:3:1 (PQ:CB:PTFE). The curves for the sample adsorbed PQ on VB cathode 4:5:1 are seen in **Figure S4**.

Grafted and absorbed PQ cells were cycled for 100 cycles at a slow rate of 10 mA g^{-1} (C/10 – C/20). This slow rate provided significant time at high and low voltages for energy storage and parasitic reactions that would affect cell capacity and stability. The discharge capacity and discharge capacity retention plots can be seen in **Figure 21** and the performance metrics of the cells after accelerated cycling can be seen in **Table 2**.

Table 2. Slow cycling performance metrics for adsorbed and grafted cathodes (PQ:CB:PTFE). Error represents standard deviation of duplicate tests, triplicate test for grafted PQ-KB.

	Initial Discharge Capacity (mAh g^{-1})	Final Discharge Capacity (mAh g^{-1})	Capacity Retention (100 cycles)	Columbic Efficiency	Round Trip Efficiency
PQ-KB (4:5:1)	158 ± 5	109 ± 5	69% ± 1%	103% ± 3%	90% ± 3%
PQ Adsorb KB (6:3:1)	166 ± 5	69 ± 5	42% ± 2%	130% ± 20%	105% ± 13%
PQ Adsorb KB (4:5:1)	210 ± 20	131 ± 8	62% ± 2%	103% ± 7%	90% ± 6%
PQ-VB (4:5:1)	154 ± 5	103 ± 4	67% ± 5%	105% ± 5%	89% ± 4%
PQ Adsorb VB (6:3:1)	140 ± 50	37 ± 7	30% ± 10%	110% ± 20%	90% ± 10%
PQ Adsorb VB (4:5:1)	139 ± 2	77 ± 3	56% ± 1%	97% ± 3%	82% ± 3%

In general, it can be seen that grafting the quinones to the carbon substrate significantly (> 5% retention) improved the stability of the ZIB cathodes when running at a slow rate that facilitates usual degradation. The slow cycling further reinforces the effect on stability that nanopore structures have on the adsorbed quinones. All the samples utilizing VB had a lower discharge capacity which is theorized to be due to the lower surface area of the VB which does not accommodate as many grafted or adsorbed quinones. With a larger ratio of KB (4:5:1), the quinones maintained a much higher capacity and stability than at a lower KB ratio (6:3:1). In fact, as a sign of instability, the CE of the PQ

adsorbed on KB 6:3:1 was significantly higher than 100% meaning substantial undercharging was occurring where degradative processes were increasing the cells discharge capacity without being reversed in the following charge.

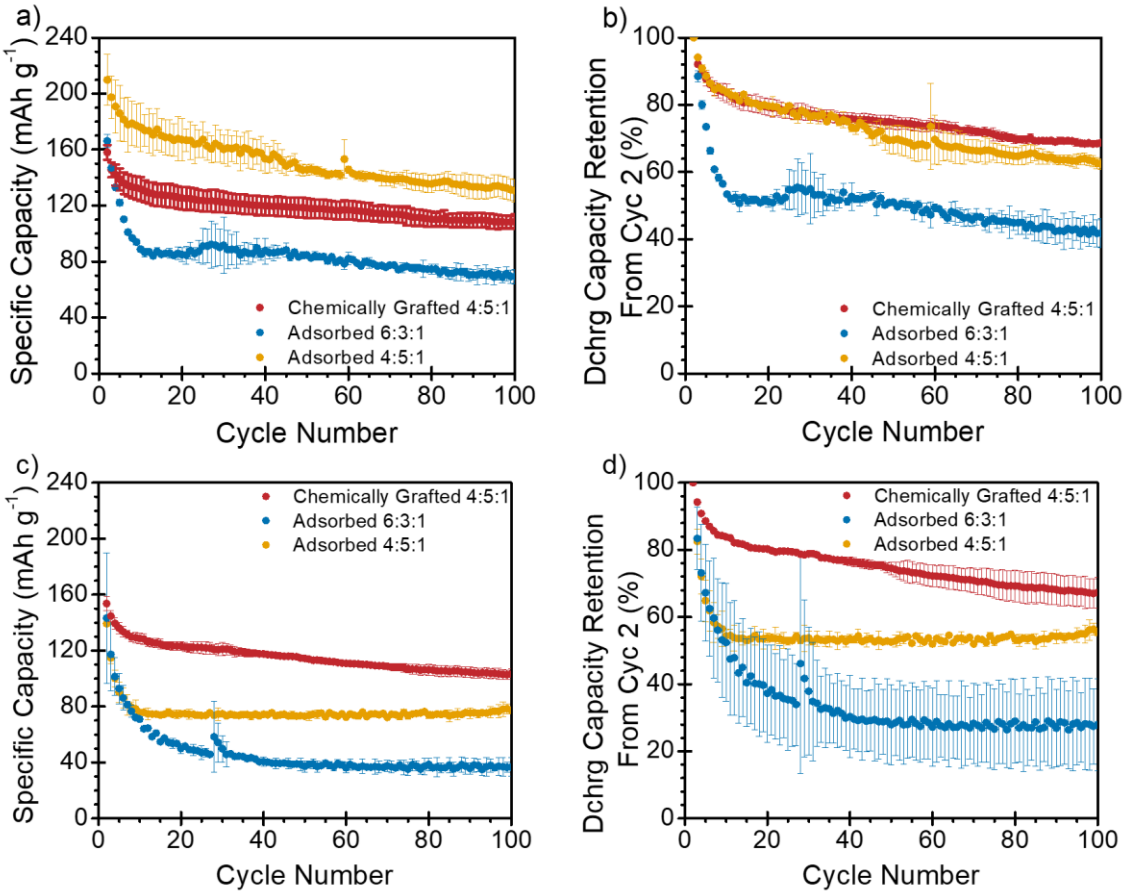

Figure 21. Slow cycling testing of cells with a current density of 10 mA g^{-1} performed on KB supported cells (top) and VB supported cells (bottom) with a) & c) showing discharge capacity, b) & d) showing discharge capacity retention. Error represents standard deviation of duplicate tests, triplicate test for grafted PQ-KB.

Although the capacity retention was highest in the grafted samples, the adsorbed quinones were stabilized by the porous structure of KB when the ratio (4:5:1) allows for

greater quinone carbon interactions rather than quinone collection on the cathode surface. However, this stabilization effect does not seem to occur when a less porous carbon black is used (VB). For context, KB is a very porous carbon black that was previously reported to have 46% of its surface area found in internal pores (< 2 nm), where less porous VB had only 30% of its surface area in internal pores [65]. The idea that adsorbed quinones perform better with appropriate quinone carbon interactions rationalizes the observed results. The best performing adsorbed sample at slow cycling had a high carbon ratio (4:5:1) on a carbon black with high surface area and high porosity (KB). The worst performing adsorbed sample at slow cycling had a high quinone 6:3:1 ratio on a carbon black with a low surface area and low porosity (VB). This sample was suspected of losing performance to quinone aggregation given its b-value and R_{CT}. Regardless, the covalently bonded quinones attached to the surface of the carbon blacks are ultimately more resilient to the degradation and aggregation forces, yielding a consistently more stable cathode.

The electrochemical GITT profiles for all the samples can be seen in **Figure 22**. The diffusion coefficient for Zn^{2+} in the ZIB cells (D) was calculated with the following equation:

$$D = \frac{4}{\pi\tau}\left(\frac{m_B V_M}{M_B S}\right)^2 \left(\frac{\Delta E_s}{\Delta E_\tau}\right)^2 \qquad \text{(Eqn. 2)}$$

Where m_B, V_M, M_B, and S are the active material mass, molar volume, active material molar mass, and cathode geometric surface area respectively. ΔE_s, ΔE_τ, and τ represent the voltage change between steady state rests, the voltage change during current pulse, and the current pulse time respectively [55], [62]. The average diffusion coefficients

were calculated to be 1.54×10^{-17} cm^2 s^{-1}, 3.82×10^{-14} cm^2 s^{-1}, and 9.85×10^{-14} cm^2 s^{-1} for the KB grafted, adsorbed 4:5:1, and adsorbed 6:3:1 samples respectively. Where the VB samples had D values of 4.33×10^{-16} cm^2 s^{-1}, 2.60×10^{-13} cm^2 s^{-1}, and 3.82×10^{-12} cm^2 s^{-1} for the grafted, adsorbed 4:5:1, and adsorbed 6:3:1 samples respectively. The grafted samples had smaller average diffusion coefficients which was expected given the increase in charge transfer resistance seen with these samples due to the interference of the grafted chains. Additionally, π-π conjugated organic cathodes, like adsorbed quinones on carbon are expected to have higher diffusion coefficients since quinones in a planar structure are expected to have lower steric hinderance of Zn^{2+} [66]. The KB samples consistently had smaller diffusion coefficients than the VB samples which makes sense given how KB has a much more porous structure.

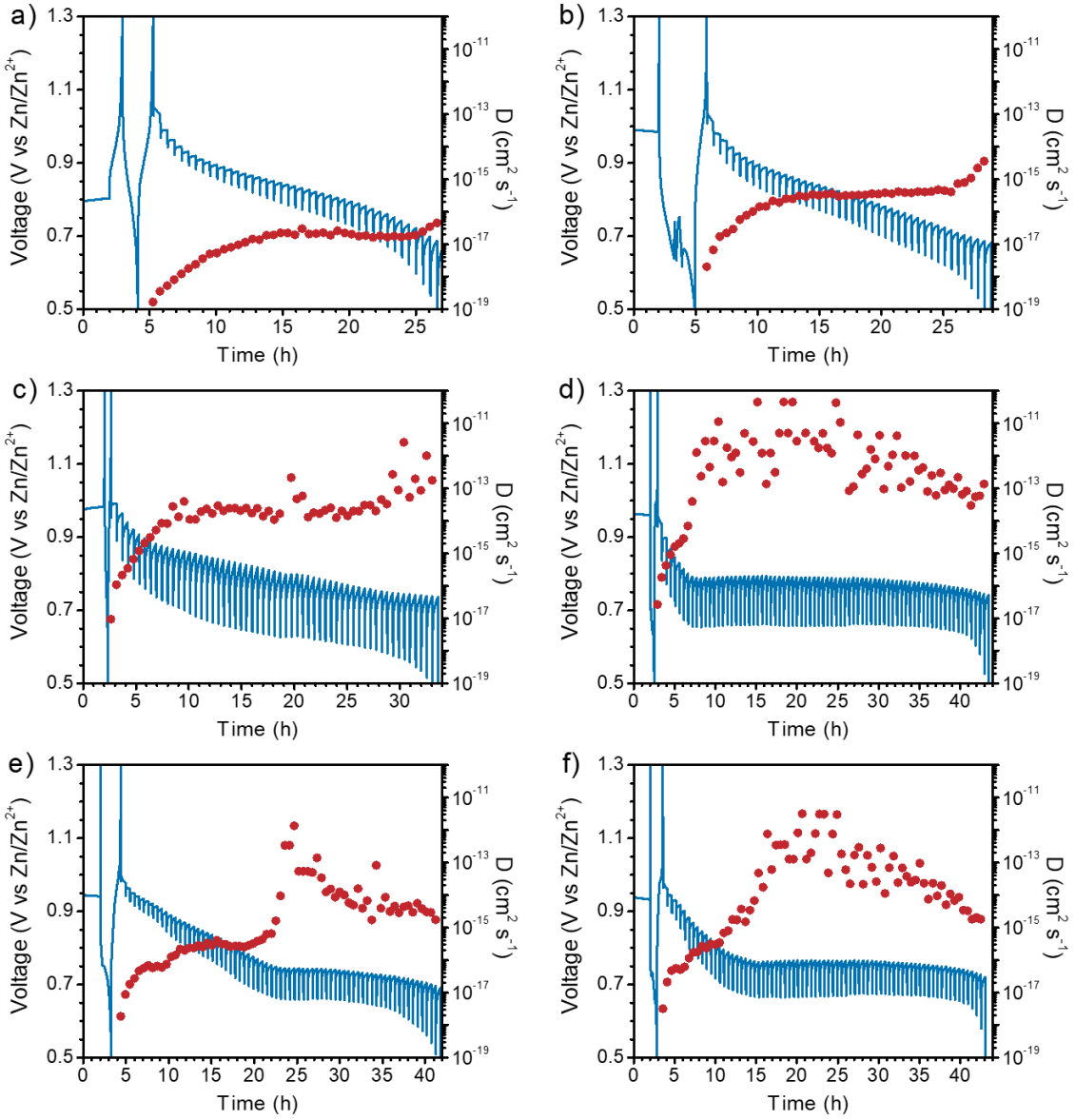

Figure 22. Galvanostatic Intermittent Titration Technique (GITT) profiles for a) chemically grafted PQ-KB 4:5:1 (PQ:CB:PTFE), b) chemically grafted PQ-VB 4:5:1, c) adsorbed PQ on KB 6:3:1, d) adsorbed PQ on VB 6:3:1, e) adsorbed PQ on KB 4:5:1, and f) adsorbed PQ on VB 4:5:1.

3.5. Conclusion

In this work, PQ was chemically grafted onto carbon black to be used as a cathode material for next-generation aqueous zinc-ion batteries. After 1000 cycles of accelerated testing the grafted PQ-KB cells achieved a capacity of 99 mAh g^{-1} (67% retention), and the grafted PQ-VB cells achieved a capacity of 91 mAh g^{-1} (71% retention). For the material ratios tested, this represents an improvement in capacity retention of at least 10% for the KB cell, and 30% for the VB cell compared to the cells with adsorbed quinones on carbon. Cells with adsorbed quinones were also stabilized more when applied with a carbon-rich ratio (4:5:1) of highly porous carbon substrate (KB). However further cycling at strictly slower rates highlighted that grafting PQ significantly improved capacity retention (5% - 37%), signalling this simple technique shows resistance to quinone inactivation for organic ZIB cathodes. This works opens the door into the application of chemical grafting for organic compounds to be used as cathode materials in ZIB. As this work focused on an initial investigation on the utility of grafting quinones for ZIB cathodes, a good next step would be to optimize the cathodic performance. There are many factors that could be optimized in synthesizing ideal grafted quinones including the grafting process, material selection, and material ratio. The grafting method used in this work is very flexible and should be expanded for investigation of new quinones and substrates. In complement to what has been noted about active material selection, this work highlights the significant impact the choice of a carbon substrate can have on cell performance. Such optimizations make the case for the commercial application of organic cathodes in ZIB stronger.

4. Conclusions and Future Work

The work outlined in this thesis presents the necessary information to understand the reasoning behind grafting organic molecules to carbon substrates and its usefulness for cathodes in ZIBs. It is clear that grafting PQ as the organic molecule of choice, made a positive impact on cell performance. Specifically, a general improvement in capacity retention was seen as the cells cycled. This improvement is related to how grafting counters a believed degradation mechanism with quinones. By fixing the location of PQ with a covalent bond, the formation of an inactivated structure of quinones is hindered as during discharge the quinones can not desorb and interact. However, this work also highlighted the importance of material ratio and carbon substrate selection in organic cathodic performance. Specifically, the use of high surface area, porous KB seems to stabilize cell capacity for adsorbed PQ more than VB. This further reinforces the idea that maintaining capacity is related to stable quinone-carbon interactions.

Building on the general findings of this project, future research can be done to optimize cell performance given the parameters available. Carbon substrate selection, an area often overlooked in the literature, seems to have a significant effect on cell performance. The previous results selection emphasized that high surface area and highly porous carbon substrates seem to stabilize adsorbed quinones. Future studies could investigate if that holds up with other high surface area carbons such as reduced graphene oxide, and carbon nanotubes. It would also be good to see if such a change affects grafted quinone stability given how the effect was small with the two carbon blacks investigated

in this study. Additionally, many organic materials could be used in diazonium grafting. Although PQ has generally been regarded as a good quinone for ZIB cathodes, other quinones should be investigated to see if they can have similar improvements with grafting. This can be applied to any quinone with an amino group capable of being converted to a diazonium salt but could be extended beyond quinones. Since diazonium grafting is done with a diazonium group on an aryl group, any other organic molecule that can incorporate these groups could in theory be grafted. This includes oligomers, polymers, and other small molecules with imine moieties. With the selection of new quinones in future work the grafting process itself can be optimized. For example, the established use of electro-grafting has shown the ability to control the grafting process to fine-tune the active material structure for the cathode. Even the current chemical grafting process could be optimized regarding the reaction time and precursor setup. Similarly, a streamlined future study would likely use commercial amino quinones to jump into the grafting investigation without the added complexity of precursor synthesis. If that can not be done, then optimizing the nitro, amino quinone synthesis reactions would be necessary for higher active material production and improving experimental throughput.

With these improvements, it would be good practice to test a large array of material ratios for the future cathodes under investigation. Using a technique like a design of experiments (DOE) could be a useful tool to locate an optimum material ratio with regard to cell performance metrics like capacity and capacity retention. In general, the use of grafting seems like a logical next step for organic cathodes in ZIBs in an effort to improve performance while maintaining the intrinsic benefits of organic cathode and ZIB design.

Given the simplicity and versatility of this modification, future work easily can and should continue to investigate its use in ZIBs.

5. References

[1] EPA, “Draft Inventory of U.S. Greenhouse Gas Emissions and Sinks 1990 - 2022,” 2024.

[2] IRENA, “World Energy Transitions Outlook 2022: 1.5°C Pathway,” Abu Dhabi, 2022.

[3] Ontario’s Independent Electricity System Operator, “Power Data: Data Directory,” 2023. [Online]. Available: https://www.ieso.ca/Power-Data/Data-Directory.

[4] Y. Shao *et al.*, “Design and Mechanisms of Asymmetric Supercapacitors,” *Chem. Rev.*, vol. 118, no. 18, pp. 9233–9280, 2018.

[5] L. E. Blanc, D. Kundu, and L. F. Nazar, “Scientific Challenges for the Implementation of Zn-Ion Batteries,” *Joule*, vol. 4, no. 4, pp. 771–799, 2020.

[6] S. W. D. Gourley, R. Brown, B. D. Adams, and D. Higgins, “Zinc-ion batteries for stationary energy storage,” *Joule*, vol. 7, no. 7, pp. 1415–1436, 2023.

[7] “DOE Global Energy Storage Database,” *Sandi National Laboratories*. [Online]. Available: https://www.energystorageexchange.org/projects/data_visualization/.

[8] D. Deng, “Li-ion batteries: basics, progress, and challenges,” *Energy Sci. Eng.*, vol. 3, no. 5, pp. 385–418, 2015.

[9] M. Brand *et al.*, “Electrical safety of commercial Li - ion cells based on NMC and NCA technology compared to LFP technology,” *World Electr. Veh. J.*, vol. 6, no.

3, pp. 572–580, 2013.

[10] G. Bhutada, “Shanghai Metals Market,” *Visual Capitalist*, 2022. [Online]. Available: https://elements.visualcapitalist.com/charted-the-most-expensive-battery-metals/.

[11] Z. A. Kader, A. Marshall, and J. Kennedy, “A review on sustainable recycling technologies for lithium-ion batteries,” *Emergent Mater.*, vol. 4, no. 3, pp. 725–735, 2021.

[12] H. Cui, L. Ma, and Z. Huang, “Organic materials - based cathode for zinc ion battery,” *SmartMat*, vol. 3, no. 4, pp. 565–581, 2022.

[13] D. Kundu, B. D. Adams, V. Du, S. H. Vajargah, and L. F. Nazar, “A high-capacity and long-life aqueous rechargeable zinc battery using a metal oxide intercalation cathode,” *Nat. Energy*, vol. 1, no. 10, 2016.

[14] O. Rubel *et al.*, “Electrochemical Stability of ZnMn2O4: Understanding Zn-Ion Rechargeable Battery Capacity and Degradation,” *J. Phys. Chem. C*, vol. 126, no. 27, pp. 10957–10967, 2022.

[15] Y. Wang *et al.*, “Electrolyte Engineering Enables High Performance Zinc-Ion Batteries,” *Small*, vol. 18, no. 43, p. 2107033, 2022.

[16] X. Liao, C. Pan, H. Yan, Y. Zhu, and Y. Pan, “Polyaniline-functionalized graphene composite cathode with enhanced Zn 2 + storage performance for aqueous zinc-ion battery,” *Chem. Eng. J.*, vol. 440, p. 135930, 2022.

[17] W. Ji, D. Du, J. Liang, G. Li, and G. Feng, “Aqueous Zn − Organic Batteries: Electrochemistry and Design Strategies,” *Batter. Energy*, vol. 2, no. 6, pp. 1–27, 2023.

[18] E. J. Son, J. H. Kim, K. Kim, and C. B. Park, “Quinone and its derivatives for energy harvesting and storage materials,” *J. Mater. Chem. A Mater. energy Sustain.*, vol. 4, pp. 11179–11202, 2016.

[19] D. M. Anjos, J. K. Mcdonough, E. Perre, G. M. Brown, S. H. Overbury, and Y. Gogotsi, “Pseudocapacitance and performance stability of quinone-coated carbon onions,” *Nano Energy*, vol. 2, no. 5, pp. 702–712, 2013.

[20] Y. Nakagawa and S. Tsujimura, “Fabrication of an Organic Redox Capacitor with a Neutral Aqueous Electrolyte Solution,” *Electrochemistry*, vol. 89, no. 3, pp. 317–322, 2021.

[21] X. Chen, H. Wang, H. Yi, and X. Wang, “Anthraquinone on Porous Carbon Nanotubes with Improved Supercapacitor Performance,” *J. Phys. Chem. C*, vol. 118, no. 16, pp. 8262–8270, 2014.

[22] H. Wang, H. Yi, C. Zhu, X. Wang, and H. Jin, “Functionalized highly porous graphitic carbon fibers for high-rate supercapacitive electrodes,” *Nano Energy*, vol. 13, pp. 658–669, 2015.

[23] Y. Liang, Z. Tao, and J. Chen, “Organic Electrode Materials for Rechargeable Lithium Batteries,” *Adv. Energy Mater.*, vol. 2, no. 7, pp. 742–769, 2012.

[24] H. Chen *et al.*, “Lithium Salt of Tetrahydroxybenzoquinone : Toward the Development of a Sustainable Li-Ion Battery,” *J. Am. Chem. Soc.*, vol. 131, no. 25, pp. 8984–8988, 2009.

[25] T. Nokami *et al.*, “Polymer-Bound Pyrene-4,5,9,10-tetraone for Fast-Charge and -Discharge Lithium-Ion Batteries with High Capacity,” *J. Am. Chem. Soc.*, vol. 134, no. 48, pp. 19694–19700, 2012.

[26] J. Kumankuma-sarpong, S. Tang, W. Guo, and Y. Fu, “Naphthoquinone-Based Composite Cathodes for Aqueous Rechargeable Zinc-Ion Batteries,” *ACS Appl. Mater. Interfaces*, vol. 13, no. 3, p. 4084−4092, 2021.

[27] K. W. Nam, H. Kim, Y. Beldjoudi, T. Kwon, D. J. Kim, and J. F. Stoddart, “Redox-Active Phenanthrenequinone Triangles in Aqueous Rechargeable Zinc Batteries,” *J. Am. Chem. Soc.*, vol. 142, no. 5, pp. 2541–2548, 2020.

[28] T. Tomai, H. Hyodo, D. Komatsu, and I. Honma, “Analysis of Degradation Mechanisms in Quinone-Based Electrodes for Aqueous Electrolyte System via In Situ XRD Measurements,” *J. Phys. Chem. C*, vol. 122, no. 5, pp. 9–14, 2018.

[29] R. Khan and Y. Nishina, “Covalent functionalization of carbon materials with redox-active organic molecules for energy storage,” *Nanoscale*, vol. 13, no. 1, pp. 36–50, 2021.

[30] M. M. Chehimi, J. Pinson, and F. Mousli, *Aryl Diazonium Salts and Related Compounds*. Cham, Switzerland: Springer Nature Switzerland AG, 2022.

[31] C. Science *et al.*, “Structure and Bonding between an Aryl Group and Metal Surfaces,” *J. Am. Chem. Soc.*, vol. 128, no. 18, pp. 6030–6031, 2006.

[32] M. P. Stewart *et al.*, “Direct Covalent Grafting of Conjugated Molecules onto Si , GaAs , and Pd Surfaces from Aryldiazonium Salts,” *J. Am. Chem. Soc.*, vol. 126, no. 1, pp. 370–378, 2004.

[33] B. D. Assresahegn, T. Brousse, and D. Bélanger, “Advances on the use of diazonium chemistry for functionalization of materials used in energy storage systems,” *Carbon N. Y.*, vol. 92, pp. 362–381, 2015.

[34] J. D. Firth and I. J. S. Fairlamb, “A Need for Caution in the Preparation and Application of Synthetically Versatile Aryl Diazonium Tetrafluoroborate Salts,” *Org. Lett.*, vol. 22, no. 18, pp. 7057–7059, 2020.

[35] A. Le Comte, T. Brousse, and D. Bélanger, “Simpler and greener grafting method for improving the stability ofanthraquinone-modified carbon electrode in alkaline media,” *Electrochim. Acta*, vol. 137, pp. 447–453, 2014.

[36] A. Le Comte, D. Chhin, A. Gagnon, R. Retoux, T. Brousse, and D. Bélanger, “Spontaneous grafting of 9,10- phenanthrenequinone on porous carbon as an active electrode material in an electrochemical capacitor in an alkaline electrolyte,” *J. Mater. Chem. A*, vol. 3, no. 11, pp. 6146–6156, 2015.

[37] I. López, S. Dabos-Seignon, and T. Breton, “Use of Selective Redox Cross-Inhibitors for the Control of Organic Layer Formation Obtained via Diazonium

Salt Reduction´," *Langmuir*, vol. 35, no. 34, pp. 11048–11055, 2019.

[38] A. Jaffe, A. S. Valdes, and H. I. Karunadasa, "Quinone-Functionalized Carbon Black Cathodes for Lithium Batteries with High Power Densities," *Chem. Mater.*, vol. 27, no. 10, pp. 3568–3571, 2015.

[39] X. Yang and A. L. Rogach, "Electrochemical Techniques in Battery Research : A Tutorial for Nonelectrochemists," *Adv. Energy Mater.*, vol. 9, no. 25, pp. 1–10, 2019.

[40] S. Fleischmann *et al.*, "Pseudocapacitance : From Fundamental Understanding to High Power Energy Storage Materials," *Chem. Rev.*, vol. 120, no. 14, pp. 6738–6782, 2020.

[41] M. Jia *et al.*, "Re-understanding the galvanostatic intermittent titration technique: Pitfalls in evaluation of diffusion coefficients and rational suggestions," *J. Power Sources*, vol. 543, p. 231843, 2022.

[42] W. Weppner and R. A. Huggins, "Determination of the Kinetic Parameters of Mixed-Conducting Electrodes and Application to the System Li3Sb," *J. Electrochem. Soc.*, vol. 124, no. 10, pp. 1569–1578, 1977.

[43] N. Elgrishi, K. J. Rountree, B. D. Mccarthy, E. S. Rountree, T. T. Eisenhart, and J. L. Dempsey, "A Practical Beginner's Guide to Cyclic Voltammetry," *J. Chem. Educ.*, vol. 95, no. 2, pp. 197–206, 2017.

[44] L. Chen *et al.*, "Hierarchical vanadium pentoxide micro flowers with excellent

long- term cyclability at high rates for lithium ion batteries," *J. Power Sources*, vol. 272, pp. 991–996, 2014.

[45] Y. Gogotsi and R. M. Penner, "Energy Storage in Nanomaterials − Capacitive, Pseudocapacitive, or Battery-like?," *ACS Nano*, vol. 12, no. 3, pp. 2081–2083, 2018.

[46] A. C. Lazanas and M. I. Prodromidis, "Electrochemical Impedance Spectroscopy - A Tutorial," *ACS Meas. Sci. Au*, vol. 3, no. 3, pp. 162–193, 2023.

[47] A. B. D. Nandiyanto, R. Oktiani, and R. Ragadhita, "How to Read and Interpret FTIR Spectroscope of Organic Material," *Indones. J. Sci. Technol.*, vol. 4, no. 1, pp. 97–118, 2019.

[48] N. Saadatkhah *et al.*, "Experimental methods in chemical engineering : Thermogravimetric analysis — TGA," *Can. J. Chem. Eng.*, vol. 98, no. 1, pp. 34–43, 2020.

[49] IEA, "Global Energy and Climate Model," Paris, 2023.

[50] N. Noor *et al.*, "Redox-Active Phenanthrenequinone Molecules and Nitrogen-Doped Reduced Graphene Oxide as Active Material Composites for Supercapacitor Applications," *ACS Omega*, vol. 9, no. 9, pp. 10080–10089, 2024.

[51] D. Kundu *et al.*, "Organic Cathode for Aqueous Zn-Ion Batteries: Taming a Unique Phase Evolution toward Stable Electrochemical Cycling," *Chem. Mater.*, vol. 30, no. 11, pp. 3874–3881, 2018.

[52] Q. Zhao *et al.*, “High-capacity aqueous zinc batteries using sustainable quinone electrodes,” *Sci. Adv.*, vol. 4, no. 3, 2018.

[53] H. Gao *et al.*, “A Pyrene-4,5,9,10-Tetraone-Based Covalent Organic Framework Delivers High Speci fi c Capacity as a Li-Ion Positive Electrode,” *J. Am. Chem. Soc.*, vol. 144, no. 21, pp. 3874–3881, 2022.

[54] H. Gao *et al.*, “Integrated Covalent Organic Framework/Carbon Nanotube Composite as Li-Ion Positive Electrode with Ultra-High Rate Performance,” *Adv. Energy Mater.*, vol. 11, no. 39, 2021.

[55] C. Guo *et al.*, “Poly(quinone-1,4-diaminoanthraquinone) cathodes for stable Zn2+ storage in aqueous zinc-ion batteries,” *Ionics (Kiel).*, vol. 29, no. 6, 2023.

[56] Y. Holade, C. Morais, K. Servat, T. W. Napporn, and K. B. Kokoh, “Enhancement of carbon supports available specific surface area for boosting the electroactivity of nanostructured Pt catalysts,” *Phys. Chem. Chem. Phys.*, vol. 16, no. 46, pp. 25609–25620, 2014.

[57] P. Kichambare, J. Kumar, S. Rodrigues, and B. Kumar, “Electrochemical performance of highly mesoporous nitrogen doped carbon cathode in lithium – oxygen batteries,” *J. Power Sources*, vol. 196, no. 6, pp. 3310–3316, 2011.

[58] C. Li *et al.*, “Alkali Metal Ion Storage of Quinone Molecules Grafted on Single-Walled Carbon Nanotubes at Low Temperature,” *ACS Omega*, vol. 3, no. 11, pp. 15598–15605, 2018.

[59] M. Toupin and D. Be, “Thermal Stability Study of Aryl Modified Carbon Black by in Situ Generated Diazonium Salt,” *J. Phys. Chem. C*, vol. 111, no. 14, pp. 5394–5401, 2007.

[60] W. Lim, X. Li, and D. Reed, “Understanding the Role of Zinc Hydroxide Sulfate and its Analogues in Mildly Acidic Aqueous Zinc Batteries : A Review,” *Small Methods*, p. 2300965, 2023.

[61] E. Laviron, “Equation Of The Peaks For A Reversible Reaction When Interactions Between The Adsorbed Molecules Are Taken Into Account,” *J. Electroanal. Chem. Interfacial Electrochem.*, vol. 52, no. 3, pp. 395–402, 1974.

[62] X. Geng *et al.*, “Long-Life Aqueous Zinc-Ion Batteries of Organic Iminodianthraquinone/rGO Cathode Assisted by Zn2+ Binding with Adjacent Molecules,” *ACS Appl. Mater. Interfaces*, vol. 14, no. 44, pp. 49746–49754, 2022.

[63] B. Yang, Y. Ma, D. Bin, H. Lu, and Y. Xia, “Ultralong-Life Cathode for Aqueous Zinc-Organic Batteries via Pouring 9 , 10-Phenanthraquinone into Active Carbon,” *ACS Appl. Mater. Interfaces*, vol. 13, no. 49, pp. 58818–58826, 2021.

[64] P. He *et al.*, “Building better zinc-ion batteries : A materials perspective,” *EnergyChem*, vol. 1, no. 3, p. 100022, 2019.

[65] J. Speder *et al.*, “Comparative degradation study of carbon supported proton exchange membrane fuel cell electrocatalysts - The influence of the platinum to carbon ratio on the degradation rate,” *J. Power Sources*, vol. 261, pp. 14–22, 2014.

[66] F. Ye *et al.*, “Organic Zinc-Ion Battery: Planar, π-Conjugated Quinone-Based Polymer Endows Ultrafast Ion Diffusion Kinetics,” *Angew. Chemie*, vol. 134, no. 51, pp. 1–8, 2022.

Appendix: Manuscript Supporting Information

Development of Stabilized Organic Cathodes via Grafting Redox-active Molecules to Carbon in Aqueous Zinc-ion Batteries for Energy Storage Systems

Thomas J. Baker [a], Alejandra Ibarra Espinoza [a], Storm W Gourley [a], Brian D. Adams [a,b], Drew Higgins [a*]

[a] Department of Chemical Engineering, McMaster University, 1280 Main Street West, Hamilton, Ontario, L8S 4L7, Canada.

[b] Salient Energy Inc., 21 McCurdy Avenue, Dartmouth, Nova Scotia, B3B 1C4, Canada.

*Corresponding author.
Email address: higgid2@mcmaster.ca (D. Higgins).

Experimental Methods: Active Material Ratio and Loadings

After grafting, the grafted material was washed with several aliquots of ethanol and vacuum filtered. The washing filtrate was recovered, and the ethanol was evaporated leaving a residue material. It was assumed that the residue is only quinone (unbonded monomers and oligomers) and that any quinone molecule not in the final product was either making up the residue or bonded to CB that did not make it to the final product (i.e., imbedded in filter paper). Thus, the calculated dried product ratio of grafted quinone to carbon was calculated by measuring the material lost during the washing process. It was found that the product was 44.2 wt% PQ. To maintain 10 wt% binder in the final cathode material 4.44 mg of PTFE was added to the 40 mg of grafted PQ-CB product for a final material ratio of 4:5:1 (PQ:CB:PTFE mass ratio).

Once the slurries were created and casted on carbon paper, the cathode active material (PQ) loadings were determined. This was done by comparing the unloaded carbon paper mass to the loaded cathode mass with the material ratios known. The loadings were normalized by the cathode geometric area (1.267 cm^2). The tested cathode samples and their respective loadings can be seen in **Table S1**.

Table S1. Six tested cathode material samples and their respective PQ loadings.

Sample and Material Weight Ratios (PQ:CB:PTFE)	**PQ Loadings (mg cm^{-2})**
Grafted PQ-KB (4:5:1)	0.43
PQ Adsorb KB (6:3:1)	0.56
PQ Adsorb KB (4:5:1)	0.51
Grafted PQ-VB (4:5:1)	0.68
PQ Adsorb VB (6:3:1)	0.95
PQ Adsorb VB (4:5:1)	0.69

Supplementary Figures

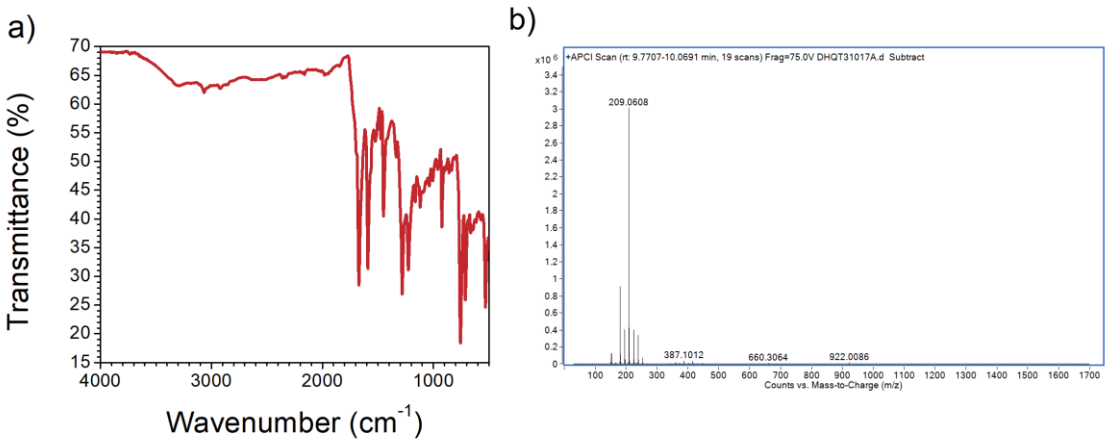

Figure S1. a) FTIR spectrogram and b) mass spectrogram of residue recovered from washing grafted PQ-KB material.

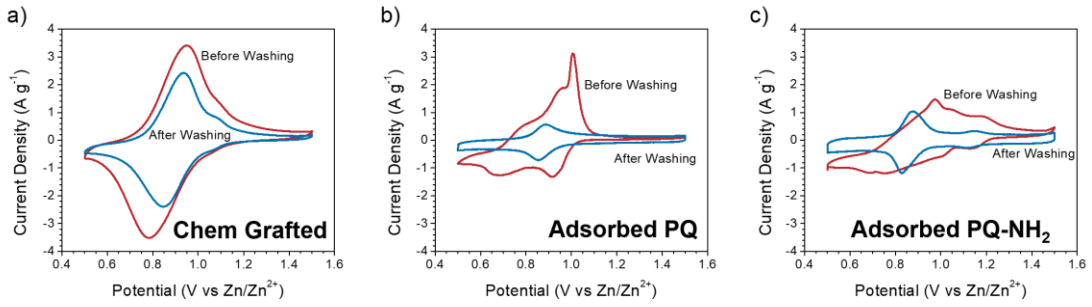

Figure S2. CV curves of crude cathode material (quinone, Vulcan black, PTFE) at 10 mV s^{-1} before solvent washing (red) and after washing (blue) for a) chemically grafted PQ, b) adsorbed PQ, e) adsorbed PQ-NH_2.

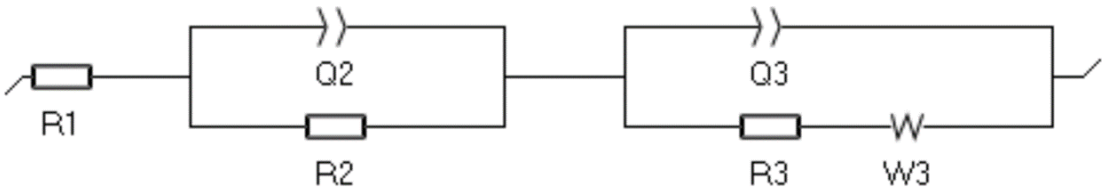

Figure S3. Equivalent model circuit for fitting EIS data. R1 represents the solution resistance, Q2 and R2 are the thin film electrolyte-electrode interface constant phase element and resistor respectively, R3 represents the R_{CT}, and Q3 and W3 are the cathode constant phase element and Warburg element respectively.

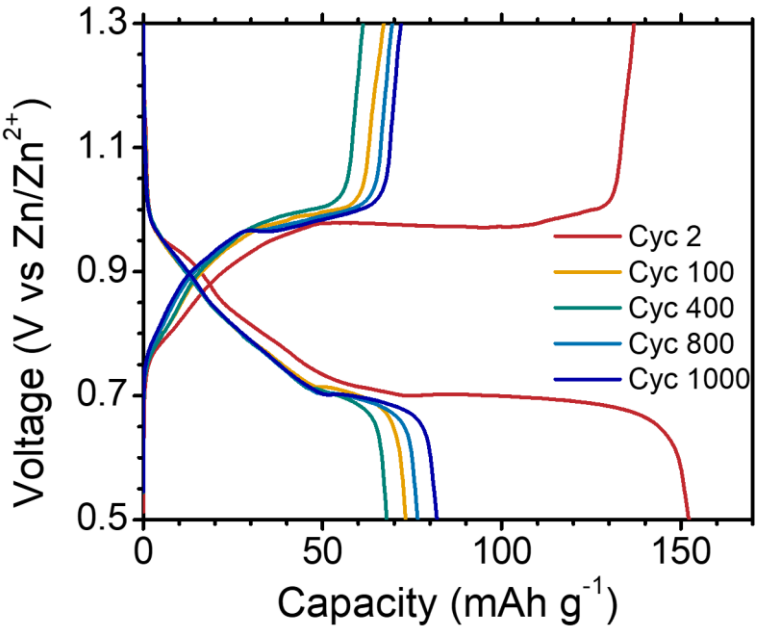

Figure S4. Charge and discharge curves for ZIBs with adsorbed PQ on VB cathode (4:5:1).

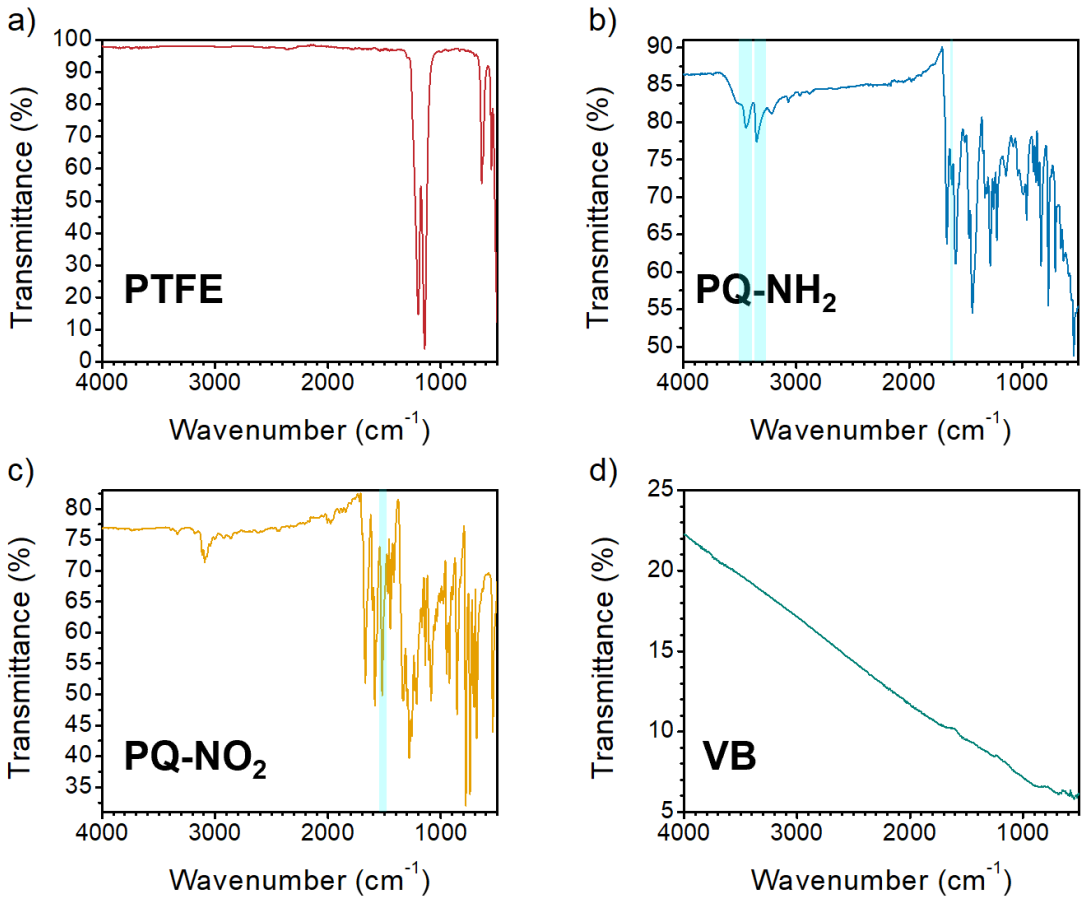

Figure S5. FTIR spectra of purified chemicals with characteristic peaks highlighted for a) PTFE, b) PQ-NH_2 (primary NH_2 stretching and bending), c) PQ-NO_2 (NO_2 stretching), d) VB.

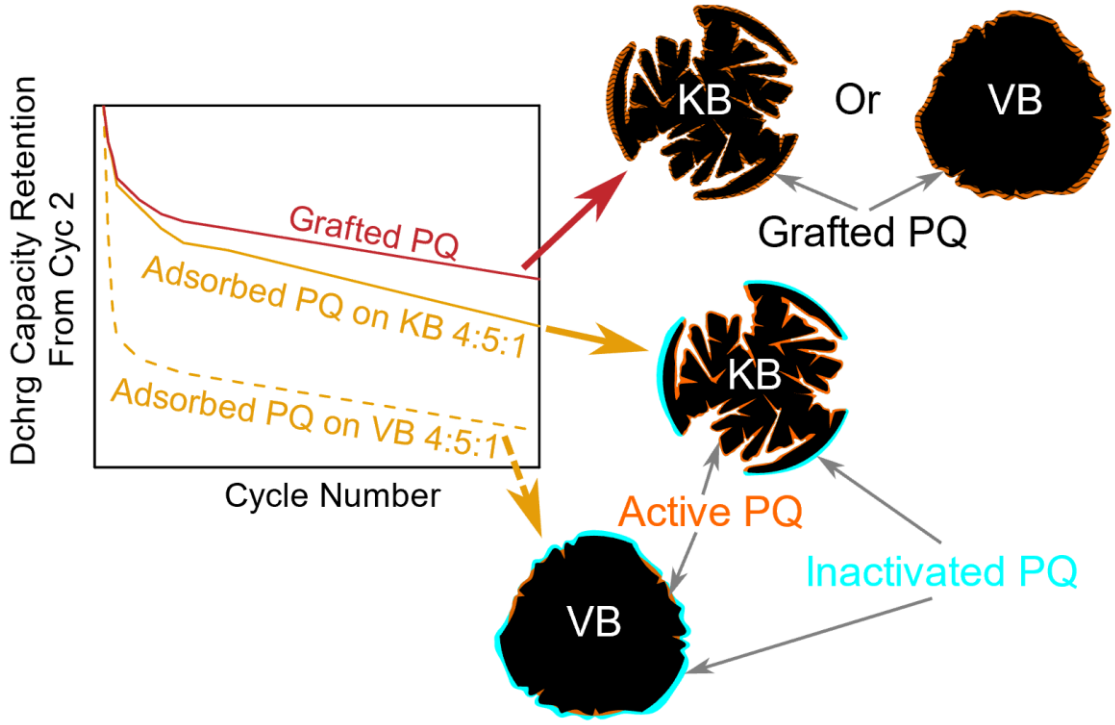

Figure S6. Diagram of capacity retention relating to PQ stabilization from grafted PQ 4:5:1 (PQ:CB:PTFE) and adsorbed PQ 4:5:1 with porous KB vs. non-porous VB carbon supports.